Journal of Molecular Liquids 308 (2020) 112983

Contents lists available at ScienceDirect

Journal of Molecular Liquids

journal homepage: www.elsevier.com/locate/molliq

Dicationic imidazolium-based dicarboxylate ionic liquids: Thermophysical properties and solubility

Bruna L. Kuhn [a], Bárbara F. Osmari [a], Thaíse M. Heinen [a], Helio G. Bonacorso [a], Nilo Zanatta [a], Steven O. Nielsen [b], Dineli T.S. Ranathunga [b], Marcos A. Villetti [c], Clarissa P. Frizzo [a,*]

[a] Department of Chemistry, Federal University of Santa Maria (UFSM), CEP 97105-900, Santa Maria, RS, Brazil
[b] Department of Chemistry and Biochemistry, University of Texas at Dallas, 800 West Campbell Road, Richardson, TX 75080, United States
[c] Lepol, Department of Physics, Federal University of Santa Maria (Universidade Federal de Santa Maria — UFSM), Santa Maria, Brazil

ARTICLE INFO

Article history:
Received 17 December 2019
Received in revised form 5 March 2020
Accepted 23 March 2020
Available online 24 March 2020

Keywords:
Ionic liquid
Dicationic
Carboxylate
Thermal
Solubility

ABSTRACT

Dicationic ionic liquids have been attracting attention due to their high thermal storage density, which is attributed to an increase in the number of cations. However, there is no information about the effect that the dianionic structure has on the thermophysical properties of dicationic ionic liquids. Thus in this study, imidazolium-based dicationic dicarboxylate ionic liquids ($C_n(MIM)_2[C_m(CO_2)_2]$, $n = 4, 6, 8, 10$ and $m = 0, 1, 2, 3, 4, 5$) were synthesized and their thermal properties were determined. The results showed that the dicarboxylate's spacer length has no effect on the melting point; however, a trend in which the heat of fusion of ionic liquids increases with the increase in the spacer chain length of the dication and dianions was observed. Moreover, dicationic dicarboxylate ionic liquids have a greater heat capacity than monocationic ionic liquids, but a smaller heat capacity than analogous dicationic ionic liquids with bromine. Our results also showed that the anion has a strong effect on the heat capacity of dicationic ionic liquids. In terms of thermal storage, $[C_6(MIM)_2][C_2]$ and $[C_6(MIM)_2][C_5]$ were the most promising ionic liquids, because they have thermal storage higher than monocationic ILs and mineral oil and compared with analogues ILs with bromine, they are potentially less toxic. All of the ionic liquids were soluble in protic polar solvents and DMSO, and were insoluble in aprotic and nonpolar–polar solvents. The study and determination of these properties is extremely important for future applications.

1. Introduction

Ionic Liquids (ILs) are classified as organic salts and the nature of these species and the possibilities for combinations among them gives them unique characteristics in terms of their physical and chemical properties, as well as their applications [1–4]. Among the most used cations, imidazolium-based ones are of greatest interest, in terms of both their synthesis and applicability. In particular, imidazolium-based dicationic ILs have interested research groups around the world, due to them being less toxic and more thermally stable than their monocationic analogs [2,5]. These ILs have emerged as strong candidates in applications such as catalysts, lubricants [6,7], surfactants [8,9], nanoparticle coatings [10], and anti-corrosion agents [11]. Dicationic ILs have been attracting attention because of their high thermal storage density [12,13], which is attributed to an increase in the number of cations, which, in turn, leads to improved charge density and, consequently, improved electrostatic energy for these ILs [12,13]. The use of carboxylate-derived anions has been widely studied recently — especially use of amino acids [14,15] and carboxylic acids [16–18], because carboxylic acids — which are obtained from a wide variety of biological sources — are environmentally friendly [17]. Some of their advantages include high heat capacity [19], water solubility [20], and antimicrobial activity [21,22]. Two examples of dicationic dianionic imidazolium-based ILs were found. The first is a family of ILs formed by citric acid and geminal dicationic imidazolium, which was reported by Aboudzadeh et al. [23]; while the second is an imidazolium-based dicarboxylate IL series — reported by Guglielmero et al. [24] — that were tested as hydrogen bond acceptors in deep eutectic mixtures. Although the number of studies on dicationic imidazolium-based ILs has increased, there are few reports in the literature on imidazolium-based dicarboxylate ILs (i.e., an anion that also has its charged portions separated by an alkyl chain).

Based on this, we postulated that by combining dicationic imidazolium-based ILs with dianionic carboxylate (Fig. 1), improved thermal properties such as thermal stability, heat capacity, and thermal storage density could be realized. Therefore, the main objective of this work is to report the synthesis, thermal properties, and solubility of

* Corresponding author.
E-mail address: clarissa.frizzo@ufsm.br (C.P. Frizzo).

https://doi.org/10.1016/j.molliq.2020.112983
0167-7322/

imidazolium-based dicationic ILs containing dicarboxylate anions. Since most of these compounds are novel, knowledge of the physical properties of these ILs is of extreme importance for future applications.

2. Experimental section

2.1. Materials

The 1,4-Bis(3-methylimidazolium-1-yl)butane bromide, 1,6-Bis (3-methylimidazolium-1-yl)hexane bromide, 1,8-Bis(3-methylimidazolium-1-yl)octane bromide, and 1,10-Bis(3-methylimidazolium-1-yl)decane bromide were synthesized in accordance with the literature [25]. AMBERLITE IRN-78 ion-exchange resin ($^{-}$OH form), oxalic acid, malonic acid, succinic acid, glutaric acid, adipic acid, pimelic acid (Sigma Aldrich, St. Louis, MO, USA), ethyl alcohol, diethyl ether, acetonitrile HPLC, methanol, ethyl acetate, propanone, dimethyl sulfoxide, chloroform, toluene, and hexane (Synth, São Paulo, Brazil) were used as received, without further purification.

2.2. Synthesis of ILs

The ILs were synthesized using the methodology described by Fukumoto et al. [26] with some modifications which is described here for $[C_4(MIM)_2][C_0]$: 1,4-Bis(3-methylimidazolium-1-yl)butane hydroxide was prepared from 1,4-Bis(3-methylimidazolium-1-yl)butane bromide ethanolic solution — using anion exchange resin — and the reaction was monitored using $AgNO_3$ 0.1 M solution. An ethanolic solution of 1,4-Bis(3-methylimidazolium-1-yl)butane hydroxide was subsequently added dropwise to an equimolar ethanolic solution of oxalic acid, and the mixture was stirred at 25 °C for 24 h. The solvent was then evaporated under reduced pressure, washed with diethyl ether (10 mL, twice), and dried under vacuum for 72 h at 60 °C. The structures of the resulting ILs were confirmed and characterized by ^{1}H and ^{13}C NMR spectroscopy, mass spectrometry, thermal analysis (TGA and DSC), and IR spectroscopy.

2.3. NMR measurements

^{1}H and ^{13}C NMR spectra were recorded on a Bruker Avance III (^{1}H at 600.13 MHz and ^{13}C at 150.03 MHz) equipped with a BCU II set to 25°C. The samples (20 mg) were placed in 5 mm tubes with 0.5 mL of DMSO-d_6 or D_2O, and a capillary containing TMS diluted in $CDCl_3$ was added as an external reference for D_2O. The NMR peak of the TMS ($\delta = 0.000$) was used as the reference in determining the ^{1}H chemical shifts in the ILs. Spectroscopic data are shown in the Supporting information.

2.4. TGA analysis

The thermal stability of the compounds was determined by a TGA Q5000 instrument (TA Instruments Inc., USA). A heating rate of 10 °C min^{-1} was used in an inert atmosphere of N_2 (25 mL min^{-1}). Samples were heated from 25 °C to: 500 °C for ILs $[C_4(MIM)_2][C_2]$, $[C_4(MIM)_2][C_5]$, $[C_6(MIM)_2][C_0]$, $[C_6(MIM)_2][C_4]$, and $[C_8(MIM)_2][C_1]$; 600 °C for ILs $[C_4(MIM)_2][C_0]$, $[C_6(MIM)_2][C_1]$, and $[C_6(MIM)_2][C_5]$; 700 °C for ILs $[C_4(MIM)_2][C_1]$, $[C_4(MIM)_2][C_3]$, $[C_4(MIM)_2][C_4]$, $[C_8(MIM)_2][C_0]$, $[C_8(MIM)_2][C_5]$, $[C_{10}(MIM)_2][C_3]$, and $[C_{10}(MIM)_2][C_5]$; 800 °C for ILs $[C_8(MIM)_2][C_2]$, $[C_8(MIM)_2][C_3]$, $[C_8(MIM)_2][C_4]$, $[C_{10}(MIM)_2][C_0]$, $[C_{10}(MIM)_2][C_1]$, $[C_{10}(MIM)_2][C_2]$, and $[C_{10}(MIM)_2][C_4]$; and 900 °C for ILs $[C_6(MIM)_2][C_2]$ and $[C_6(MIM)_2][C_3]$. The calibration of equipment was checked with $CaC_2O_4{\cdot}H_2O$ (99.9%), and the sample mass was 1–5 mg. Before the heating ramp, an isotherm of 120 °C was performed for 30 min in order to minimize the interference of the residual water on the sample. The data were treated using version 4.5 of the TA Universal Analysis 2000 Software (TA Instruments Inc., USA). The volatile content values were taken from the TGA curves without isotherm for all ILs.

2.5. DSC analysis

The phase transitions were obtained by Differential Exploratory Calorimetry of Modulated Temperature, using a Q2000 DSC calorimeter (TA Instruments, USA) equipped with an RCS refrigeration accessory and N_2 as purge gas (50 mL min^{-1}). The heating rate used was 5 °C min^{-1}. The calibration of instrument in standard DSC mode was verified with indium (99.99%). The masses of the reference and sample pans with lids were measured and shown to be 51 ± 0.02 mg. Samples were sealed in aluminum pans with hermetic lids, with one hole therein for release of water. The masses of the samples (1–5 mg) were weighed on a Sartorius balance (M500P) with precision of ±0.001 mg. Before the first cycle, an isotherm of 120 °C was performed for 30 min in order to eliminate residual water from the sample. All samples were subjected to three heating-cooling cycles, as follows: −80 to 130 °C for IL $[C_4(MIM)_2][C_1]$; −80 to 140 °C for IL $[C_{10}(MIM)_2][C_1]$; −80 to 150 °C for ILs $[C_4(MIM)_2][C_2]$ and $[C_{10}(MIM)_2][C_0]$; −80 to 160 °C for ILs $[C_8(MIM)_2][C_0]$ and $[C_8(MIM)_2][C_1]$; −80 to 170 °C for ILs $[C_6(MIM)_2][C_1]$, $[C_6(MIM)_2][C_2]$, and $[C_{10}(MIM)_2][C_4]$; −80 to 180 °C for ILs $[C_4(MIM)_2][C_3]$, $[C_4(MIM)_2][C_4]$, $[C_4(MIM)_2][C_5]$, $[C_6(MIM)_2][C_3]$, $[C_6(MIM)_2][C_4]$, $[C_8(MIM)_2][C_2]$, $[C_8(MIM)_2][C_4]$, $[C_{10}(MIM)_2][C_2]$, $[C_{10}(MIM)_2][C_3]$, and $[C_{10}(MIM)_2][C_5]$; −80 to 190 °C for IL $[C_8(MIM)_2][C_3]$; and −80 to 200 °C for ILs $[C_4(MIM)_2][C_3]$, $[C_6(MIM)_2][C_0]$, $[C_6(MIM)_2][C_5]$, and $[C_8(MIM)_2][C_5]$. The data were treated using version 4.5 of the TA Universal Analysis 2000 Software (TA Instruments Inc., USA). Isothermal Annealing Experiments: First, an isotherm at 120 °C for 30 min was performed. Sample was heated from −80 to 180 °C at a heating rate of 10 °C min^{-1}. After annealing at 180 °C (30 min), sample was cooling from 180 to −80 °C at a rate of 1 °C min^{-1} and a second heating cycle was performed.

2.6. Heat capacity

For the determination of heat capacities (C_p), samples were sealed in aluminum pans with hermetic lids. The lids and pans (reference and sample) weighed about 52 ± 0.02 mg. The masses of the samples (7–8 mg) were weighed on a Sartorius balance (M500P) with precision of ±0.001 mg. In this study, the heat capacities determined relative to that of liquid water were measured and compared to the data of Osborne et al. [27,28] (Table S4). Based on comparison with literature values for water, the uncertainty of the C_p measurements is estimated to be ±9%. Scans for water and ILs were obtained from the heat capacities between 298.15 and 348.15 K. However, the data used were between 314.15 and 343.15 K for the ILs. The temperature program chosen for the determination of C_p consisted of an isothermal segment of 15 min at 298.15 K followed by a constant heating rate of 5 K·min^{-1} to 348.15 K, at which point the temperature was held using an isothermal segment of 15 min. The C_p for each IL was determined by an average of three runs, and the standard deviation is available in the ESI.

2.7. ESI-MS analysis

ESI-MS-MS were acquired with an Agilent Technologies 6460 Triple Quadruple mass spectrometer (LC-MS-MS) (Santa Clara, CA, USA), operating in the positive and negative ion mode. The gas temperature was 300 °C, and the dry gas flow was 5 L min^{-1}. The nebulizer remained at 45 psi. The capillary voltage was 3500 V and the shredder voltage was 3 V. The IL solutions in water were introduced at a flow rate of 5 μL min^{-1}. Nitrogen was used as both the nebulizer and the collision gas. Molecular ions were detected using the positive and negative mode, in which the m/z ratio is given for a dication and an anion, or

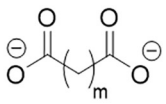	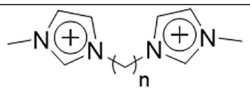			
	n = 4	n = 6	n = 8	n = 10
m= 0	$[C_4(MIM)_2][C_0]$	$[C_6(MIM)_2][C_0]$	$[C_8(MIM)_2][C_0]$	$[C_{10}(MIM)_2][C_0]$
m = 1	$[C_4(MIM)_2][C_1]$	$[C_6(MIM)_2][C_1]$	$[C_8(MIM)_2][C_1]$	$[C_{10}(MIM)_2][C_1]$
m = 2	$[C_4(MIM)_2][C_2]$	$[C_6(MIM)_2][C_2]$	$[C_8(MIM)_2][C_2]$	$[C_{10}(MIM)_2][C_2]$
m = 3	$[C_4(MIM)_2][C_3]$	$[C_6(MIM)_2][C_3]$	$[C_8(MIM)_2][C_3]$	$[C_{10}(MIM)_2][C_3]$
m = 4	$[C_4(MIM)_2][C_4]$	$[C_6(MIM)_2][C_4]$	$[C_8(MIM)_2][C_4]$	$[C_{10}(MIM)_2][C_4]$
m = 5	$[C_4(MIM)_2][C_5]$	$[C_6(MIM)_2][C_5]$	$[C_8(MIM)_2][C_5]$	$[C_{10}(MIM)_2][C_5]$

Fig. 1. Imidazolium-based dicarboxylate ILs synthesized in this work.

only for an anion. Anionic aggregates were detected only in the negative mode.

2.8. IR analysis

The infrared absorption spectra were recorded as KBr pellets - with 45 scans and a reading range between 400 and 4500 cm^{-1} - on a Shimadzu IR Prestige Fourier Transform Infrared Spectroscopy spectrophotometer.

2.9. Bromide content

For the determination of bromine ions, the volumetric precipitation method was used, together with a bromine selective-ion electrode (ISE Br, United States, imported by Marte Científica, Brazil.). A 25 mg amount of the IL was diluted in 50 mL of deionized water and titrated with 0.1 M of $AgNO_3$ solution. The reaction was monitored through the formation of a white precipitate of AgBr and through the equivalence point accompanied by the bromine selective-ion electrode.

2.10. Density

Calibration of the pycnometer (5 mL) was performed with Millipore water with double and deionized distillation (Elix-03, Barueri, Brazil; and Milli-Q, Molsheim, France). The measurements of the relative density of ILs was determined at 298 ± 0.5 K and hexane was used (Synth, São Paulo, Brazil), as a non-solvent. An analytical balance (0.0001 g precision) (Weblabor, São Paulo, Brazil) was used for the measurements of the masses of ILs and hexane.

2.11. Computational details

We analyze the density and the heat capacity of four selected ionic liquids, namely $[C_4(MIM)_2][C_5]$, $[C_4(MIM)_2][C_1]$, $[C6(MIM)_2][C_5]$ and $[C_6(MIM)_2][C_1]$ using molecular dynamics (MD) computer simulations. All the MD simulations were conducted using the NAMD software package (v.2.13) [29]. Both the pimelate and malonate anions were represented using the CHARMM general force field (CGenFF). The $[C_4(MIM)_2]^{2+}$ and $[C_6(MIM)_2]^{2+}$ cation parameters were obtained from Gross et al. [30]. We also calculated the properties of pure water using the TIP3P water model. [31] Even though the transport properties measured in simulations with a polarizable force field show better agreement with experiments, [32] it is prohibitively expensive to use in ionic liquid studies. [33] With a non-polarizable model, one of the well-known methods to account for the polarization and charge transfer effects in ionic liquids is by scaling the atomic charges. [33] In several studies it is reported that a 0.8 scaling factor can accurately predict the known experimental density and heat capacity values of imidazolium based ionic liquids. [31,33–37] Hence, we scaled the atomic partial charges of the ionic liquids by 0.8 in the current study. The ionic liquid systems containing 250 ion pairs each were randomly placed in a 50 × 50 × 50 $Å^3$ cubic box using Packmol [38] and periodic boundary conditions were applied in all three directions. To equilibrate the systems, first a canonical (NVT) simulation was conducted for 10 ns at 300 K. Since the ionic liquids show slow dynamics, to get rid of any energy traps and to mix the molecules thoroughly an annealing simulation was done by heating the system up to 700 K [33–37] and cooling stepwise in 10 K increments to the target temperature over 10 ns in the isobaric—isothermal (NPT) ensemble at a pressure of 1 atm. Then a 200 ns long NPT run was performed at 300 K and 1 atm. The densities were computed from an average of the last 60 ns of this 200 ns run. The heat capacity was analyzed by running twelve different independent NPT simulations for each system starting from the previous configuration, each for 30 ns, over a selected temperature range. Considering the temperatures used for the experimental analysis, systems with $[BisBut(MIM)_2]^{2+}$ ions were simulated at temperatures ranging from 315.0 to 342.5 K, systems with $[BisHex(MIM)_2]^{2+}$ ions were simulated from 305.0 to 332.5 K and the water system was simulated at temperatures ranging from 308.0 to 335.5 K. The last 15 ns of the trajectories were considered to compute the average heat capacities. Following the definition in Cadena et al. (Eq. (1)) and assuming the heat capacity as a constant over the selected small temperature range, the heat capacity at constant pressure was determined from the slope of the enthalpy versus temperature graph (see Figs. S208–S211).

$$C_P(T,P) = \left(\frac{\partial\langle H\rangle}{\partial T}\right)_P = \left(\frac{\partial\langle H_{res}\rangle}{\partial T}\right)_P + \left(\frac{\partial\langle H_{ig}\rangle}{\partial T}\right)_P \quad (1)$$

In Eq. (1), $H_{res} = \Phi^{NB} + PV - Nk_BT$ represents the residual portion of the heat capacity, which takes into account all the nonbonded interactions and $H_{ig} = \Phi^{INT} + KE + Nk_BT$ is the ideal gas contribution that accounts for intramolecular interactions. [38] Even though both contributions can be calculated using classical MD simulations, generally the ideal gas portion is taken from experiments or estimated from ab-initio frequency analysis (because the values calculated from classical MD can be significantly higher than the experimental data). [34,38] Since the results we obtained from the classical force fields show a fair agreement to the experiments (% error < 10), we have not seen the need to calculate the ideal gas portion of the heat capacity using quantum mechanical calculations. But by replacing the ideal gas portion (see table S6) obtained from classical MD with a quantum mechanical estimation, more accurate heat capacities should be obtainable. [38]

2.12. Solubility

The solubility of the studied ILs was determined, as defined in Vogel's *Textbook of Practical Organic Chemistry* [39]. Popular representative solvents were chosen and ranked in descending order of their Snyder polarity index value: water, 9.0; methanol, 6.6; DMSO, 6.5; acetonitrile, 6.2; acetone, 5.1; ethanol, 5.1; ethyl acetate, 4.4; isopropyl alcohol, 4.3; chloroform, 4.1; toluene, 2.3; and hexane, 0.0. A 0.1 g

amount of each IL was dissolved and characterized as follows: good solubility when dissolved in 1 mL of the solvent; medium solubility when dissolved in 3 mL of the solvent; poor solubility when not dissolved in 3 mL. Solubility was conducted at 25 °C under ambient pressure.

2.13. Spectral data

1,4-Bis(3-methylimidazol-1-yl)butane Oxalate $[C_4(MIM)_2][C_0]$: $C_{14}H_{20}N_4O_4$, MW: 308.33 g·mol^{-1}; Pale yellow solid; 89%, T_g: -7.33 °C; ^{1}H NMR (600.13 MHz, D_2O): δ 8.71 (s, 2H, 2CH); 7.45 (s, 2H, 2CH); 7.41 (s, 2H, 2CH); 4.22–4.21 (m, 4H, $2CH_2$); 3.86 (s, 6H, $2CH_3$); 1.89–1.87 (m, 4H, $2CH_2$). ^{13}C NMR (150.32 MHz, D_2O): δ 167.06 ($2COO^-$); 136.19 (2CH); 123.96 (2CH); 126.31 (2CH); 48.95 ($2CH_2$); 35.97($2CH_3$); 26.43 ($2CH_2$). MS *m/z* molecular ion: 309.20 (cation), 89.10 (anion). IR (KBr, ν/cm^{-1}): 3147, 3078, 2954, 2865, 1595, 1576, 1456, 1167, 786, 622. Volatile content: 11%. Bromide content: 16 ppm.

1,4-Bis(3-methylimidazol-1-yl)butane malonate $[C_4(MIM)_2][C_1]$ [24]: $C_{15}H_{22}N_4O_4$; MW: 322.3596 g·mol^{-1}; Viscous liquid pale yellow; 80%, T_g: -0.78 °C; ^{1}H NMR (600.13 MHz, $DMSO_{d6}$): δ 9.71 (s, 2H, 2CH); 7.77 (s, 2H, 2CH); 7.65 (s, 2H, 2CH); 4.30–4.28 (m, 4H, $2CH_2$); 3.87 (s, 6H, $2CH_3$); 2.75 (s, 2H, $2CH_2$); 1.79–1.76 (m, 4H, $2CH_2$). ^{13}C NMR (150.32 MHz, $DMSO_{d6}$): δ 172.41 ($2COO^-$); 137.26 (2CH); 123.61 (2CH); 122.24 (2CH); 47.75 ($2CH_2$); 35.77 ($2CH_3$); 25.95 ($2CH_2$), (CH_2 relative to the malonate shows the same chemical shift as $DMSO_{d6}$). MS *m/z* molecular ion: 323.00 (cation), 103.00 (anion). IR (KBr, ν/cm^{-1}): 3147, 3088, 3084, 2955, 2868, 2049, 1573, 1457, 1167, 788, 622. Volatile content: 20%. Bromide content: 16 ppm.

1,4-Bis(3-methylimidazol-1-yl)butane succinate $[C_4(MIM)_2][C_2]$ [24]: $C_{16}H_{24}N_4O_4$; MW: 336.3862 g·mol^{-1}; white solid; 94%, T_{g1}: −29.35 °C; T_{g2}: - 4.6 °C; ^{1}H NMR (600.13 MHz, $DMSO_{d6}$): δ 9.31 (s, 2H, 2CH); 7.85–7.84 (m, 2H, 2CH); 7.77–7.76 (m, 2H, 2CH); 4.28–4.26 (m, 4H, $2CH_2$); 3.88 (s, 6H, $2CH_3$); 2.29 (s, 4H, $2CH_2$); 1.82–1.80 (m, 4H, $2CH_2$). ^{13}C NMR (150.32 MHz, $DMSO_{d6}$): δ 175.27 ($2COO^-$); 136.70 (2CH); 123.65 (2CH); 122.25 (2CH); 47.95 ($2CH_2$); 35.82 ($2CH_3$); 32.02 ($2CH_2$); 26.07 ($2CH_2$). MS *m/z* molecular ion: 337.20 (cation), 117.10 (anion). IR (KBr, ν/cm^{-1}): 3151, 3100, 2964, 2938, 1573, 1464, 1167, 756, 622. Volatile content: 6%. Bromide content: 43 ppm.

1,4-Bis(3-methylimidazol-1-yl)butane glutarate $[C_4(MIM)_2][C_3]$ [24]: $C_{17}H_{26}N_4O_4$; MW: 350.4127 g·mol^{-1}; pale yellow solid; 92%, T_g: 2.5 °C; ^{1}H NMR (600.13 MHz, $DMSO_{d6}$): δ 10.19 (s, 2H, 2CH); 7.94 (s, 2H, 2CH); 7.75 (s, 2H, 2CH); 4.31–4.29 (m, 4H, $2CH_2$); 3.88 (s, 6H, $2CH_3$); 1.88 (t, J = 7.45 Hz, 4H, $2CH_2$); 1.79–1.77 (m, 4H, $2CH_2$); 1.60 (qui, J = 7.35, 2H, CH_2). ^{13}C NMR (150,32 MHz, $DMSO_{d6}$): δ 177.08 ($2COO^-$); 137.30 (2CH); 123.62 (2CH); 122.28 (2CH); 47.97 ($2CH_2$); 38.17 ($2CH_2$); 35.76 ($2CH_3$); 26.07 ($2CH_2$); 23.33 (CH_2). MS *m/z* molecular ion: 351.10 (cation), 131.10 (anion). IR (KBr, ν/cm^{-1}): 3154, 3107, 2963, 2919, 1566, 1449, 1168, 742, 622. Volatile content: 8%. Bromide content: 11 ppm.

1,4-Bis(3-methylimidazol-1-yl)butane Adipate $[C_4(MIM)_2][C_4]$: $C_{18}H_{28}N_4O_4$; MW: 364.4393 g·mol^{-1}; pale yellow solid; 93%, T_{g1}: −25.1 °C; T_{g2}: 2.0 °C; ^{1}H NMR (600.13 MHz, $DMSO_{d6}$): δ 10.28–10.27 (m, 2H, 2CH); 7.95 (s, 2H, 2CH); 7.76 (s, 2H, 2CH); 4.32–4.29 (m, 4H, $2CH_2$); 3.88 (s, 6H, $2CH_3$); 1.83–1.80 (m, 4H, $2CH_2$); 1.79–1.77 (m, 4H, $2CH_2$); 1.38–1.36 (m, 4H, $2CH_2$). ^{13}C NMR (150.32 MHz, D_2O): δ 183.25 ($2COO^-$); 136.20 (2CH); 123.98 (2CH); 122.29 (2CH); 48.93 ($2CH_3$); 37.24 ($2CH_2$); 35.92 ($2CH_3$); 26.42 ($2CH_2$); 25.89 ($2CH_2$). MS *m/z* molecular ion: 365.20 (cation), 145.10 (anion). IR (KBr, ν/cm^{-1}): 3151, 3096, 2932, 2862, 1570, 1458, 1167, 741, 621. Volatile content: 7%. Bromide content: 2 ppm.

1,4-Bis(3-methylimidazol-1-yl)butane pimelate $[C_4(MIM)_2][C_5]$: $C_{19}H_{30}N_4O_4$; MW: 378.4659 g·mol^{-1}; white solid; 92%, T_g: −13.3 °C; ^{1}H NMR (600.13 MHz, $DMSO_{d6}$): δ 9.46 (s, 2H, 2CH); 7.87 (s, 2H, 2CH); 7.77 (s, 2H, 2CH); 4.29–4.27 (s, 4H, $2CH_2$); 3.89 (s, 6H, $2CH_3$); 2.04 (t, J = 7.4 Hz, 4H, $2CH_2$); 1.83–1.81 (m, 4H, $2CH_2$); 1.42 (qui, J = 7.5 Hz, 4H, $2CH_2$); 1.22–1.16 (m, 2H, CH_2). ^{13}C NMR (150.32 MHz, $DMSO_{d6}$): δ 176.08 ($2COO^-$); 136.91 (2CH); 123.62 (2CH); 122.25 (2CH); 47.86 ($2CH_2$); 35.90 ($2CH_2$); 35.79 ($2CH_3$); 28.94 ($2CH_2$); 26.03 ($2CH_2$); 25.35 (2CH). MS *m/z* molecular ion: 379.20 (cation), 159.10 (anion). IR (KBr, ν/cm^{-1}): 3153, 3102, 2942, 2885, 1571, 1463, 1167, 754, 620. Volatile content: 8%, Bromide content: 62 ppm.

1,6-Bis(3-methylimidazol-1-yl)hexane Oxalate $[C_6(MIM)_2][C_0]$: $C_{16}H_{24}N_4O_4$; MW: 336.3862 g·mol^{-1}; white solid; 97%, T_{g1}: −29.5 °C; T_{g2}: 21.04 °C; ^{1}H NMR (600.13 MHz, $DMSO_{d6}$): δ 9.81 (s, 2H, 2CH); 7.81 (s, 2H, 2CH); 7.69 (s, 2H, 2CH); 4.20 (t, J = 7.2, 4H, $2CH_2$); 3.88 (s, 6H, $2CH_3$); 1.78–1.76 (m, 4H, $2CH_2$); 1.27–1.25 (m, 4H, $2CH_2$). ^{13}C NMR (150.32 MHz, $DMSO_{d6}$): δ 170.07 ($2COO^-$); 137.73 (2CH); 123.45 (2CH); 122.16 (2CH); 48.35 ($2CH_2$); 35.67 ($2CH_3$); 28.96 ($2CH_2$); 24.40 ($2CH_2$). MS *m/z* molecular ion: 337.40 (cation), 89.00 (anion). IR (KBr, ν/cm^{-1}): 3153, 3099, 2940, 2863, 1600, 1462, 1168, 774, 622. Volatile content: 0% (TGA). Bromide content: 20 ppm.

1,6-Bis(3-methylimidazol-1-yl)hexane malonate $[C_6(MIM)_2][C_1]$ [24]: $C_{17}H_{26}N_4O_4$; MW: 350.4127 g·mol^{-1}; pale yellow oil; 81%, T_g: -9.36 °C; ^{1}H NMR (600.13 MHz, $DMSO_{d6}$): δ 9.34 (s, 2H, 2CH); 7.87 (s, 2H, 2CH); 7.78 (s, 2H, 2CH); 4.21 (t, J = 7.2 Hz, 4H, $2CH_2$); 3.90 (s, 6H, $2CH_3$); 2.75 (s, 2H, $2CH_2$); 1.83–1.79 (m, 4H, $2CH_2$); 1.30–1.28 (m, 4H, $2CH_2$); ^{13}C NMR (150.32 MHz, $DMSO_{d6}$): δ 171.61 ($2COO^-$); 136.53 (2CH); 123.54 (2CH); 122.24 (2CH); 48.56 (2CH2); 38.89 ($2CH_2$); 35.77($2CH_3$); 29.08 ($2CH_2$); 24.77 ($2CH_2$). MS *m/z* molecular ion: 351.30 (cation), 103.00 (anion). IR (KBr, ν/cm^{-1}): 3152, 3101, 2941, 2864, 1571, 1464, 1168, 759, 621. Volatile content: 19% (TGA). Bromide content: 2 ppm.

1,6-Bis(3-methylimidazol-1-yl)hexane succinate $[C_6(MIM)_2][C_2]$ [24]: $C_{18}H_{28}N_4O_4$; MW: 364.4393 g·mol^{-1}; white solid; 87%, T_g: -1.02 °C; ^{1}H NMR (600.13 MHz, $DMSO_{d6}$): δ 9.64–9.62 (m, 2H, 2CH); 7.83 (s, 2H, 2CH); 7.73 (s, 2H, 2CH); 4.19 (t, J = 7.111 Hz, 4H, 2CH2); 3.87 (s, 6H, $2CH_3$); 2.19 (s, 4H, $2CH_2$); 1.79–1.76 (m, 4H, $2CH_2$); 1.28–1.25 (m, 4H, $2CH_2$); ^{13}C NMR (150.32 MHz, $DMSO_{d6}$): δ 176.09 ($2COO^-$); 137.28 (2CH); 123.54 (2CH); 122.25 (2CH); 48.52 ($2CH_2$); 35.68 ($2CH_3$); 33.99 ($2CH_2$); 29.09 ($2CH_2$); 24.73 ($2CH_2$). MS *m/z* molecular ion: 365.40 (cation), 117.00 (anion). IR (KBr, ν/cm^{-1}): 3151, 31,011, 2964, 2938, 2862, 1512, 1465, 1413, 1168, 766, 642, 547. Volatile content: 13% (TGA). Bromide content: 17 ppm.

1,6-Bis(3-methylimidazol-1-yl)hexane glutarate $[C_6(MIM)_2][C_3]$ [24]: $C_{19}H_{30}N_4O_4$; MW: 378.4659 g·mol^{-1}; pale yellow oil; 91%, T_g: -10.78 °C; ^{1}H NMR (600.13 MHz, $DMSO_{d6}$): δ 9.68 (s, 2H, 2CH); 7.86 (s, 2H, 2CH); 7.75 (s, 2H, 2CH); 4.19 (t, J = 7.17 Hz, 4H, $2CH_2$); 3.88 (s, 6H, $2CH_3$); 1.99 (t, J = 7.35 Hz, 4H, $2CH_2$); 1.81–1.76 (m, 4H, $2CH_2$); 1.62 (qui, J = 7.34 Hz, 2H, CH_2); 1.28–1.25 (m, 4H, $2CH_2$); ^{13}C NMR (150.32 MHz, $DMSO_{d6}$): δ 176.27 ($2COO^-$); 137.27 (2CH); 123.54 (2CH); 122.29 (2CH); 48.52 ($2CH_2$); 37.21 ($2CH_2$); 35.67 ($2CH_3$); 29.12 ($2CH_2$); 24.76 ($2CH_2$); 22.71 (CH_2); MS *m/z* molecular ion: 379.40 (cation), 131.00 (anion). IR (KBr, ν/cm^{-1}): 3153, 3102, 2963, 2863, 1569, 1449, 1168, 742, 622. Volatile content: 9%. Bromide content: 18 ppm.

1,6-Bis(3-methylimidazol-1-yl)hexane Adipate $[C_6(MIM)_2][C_4]$: $C_{20}H_{32}N_4O_4$; MW: 392.4925 g·mol^{-1}; pale yellow oil; 82%, T_g: -7.06 °C; ^{1}H NMR (600.13 MHz, $DMSO_{d6}$): δ 9.77 (s, 2H, 2CH); 7.82–7.82 (m, 2H, 2CH); 7.71–7.70 (m, 2H, 2CH); 4.18 (t, J = 7.2 Hz, 4H, $2CH_2$); 3.87 (s, 6H, $2CH_3$); 1.87–1.85 (m, 4H, $2CH_2$); 1.79–1.77 (m, 4H, $2CH_2$); 1.39–1.36 (m, 4H, $2CH_2$); 1.27–1.25 (m, 4H, $2CH_2$); ^{13}C NMR (150.32 MHz, $DMSO_{d6}$): δ 176.05 ($2COO^-$); 137.42 (2CH); 123.47 (2CH); 122.24 (2CH); 48.50 ($2CH_2$); 38.30 ($2CH_2$); 35.66 ($2CH_3$); 29.09 ($2CH_2$); 26.64 ($2CH_2$); 24.76 ($2CH_2$); MS *m/z* molecular ion: 393.40 (cation), 145.00 (anion). (KBr, ν/cm^{-1}): 3152, 3102, 2943, 2922, 2867, 1571, 1460, 1169, 735, 622. Volatile content: 18%. Bromide content: 14 ppm.

1,6-Bis(3-methylimidazol-1-yl)hexane pimelate: $C_{21}H_{34}N_4O_4$; MW: 406.5191 g·mol^{-1}; pale yellow solid; 94%, T_g: −18.16 °C; ^{1}H NMR (600.13 MHz, $DMSO_{d6}$): δ 9.67 (s, 2H, 2CH); 7.81 (s, 2H, 2CH); 7.70 (s, 2H, 2CH); 4.18 (t, J = 7.28 Hz, 4H, $2CH_2$); 3.87 (s, 6H, $2CH_3$); 1.86–1.85 (m, 4H, $2CH_2$); 1.79–1.76 (m, 4H, $2CH_2$); 1.40–1.34 (m, 4H, $2CH_2$); 1.28–1.25 (m, 4H, 2CH2); 1.16–1.12 (m, 2H, CH_2); ^{13}C NMR

(150.32 MHz, $DMSO_{d6}$): δ 176.33 ($2COO^-$); 137.36 (2CH); 123.55 (2CH); 122.28 (2CH); 48.57 ($2CH_2$); 38.29 ($2CH_2$); 35.70 ($2CH_3$); 29.86 ($2CH_2$); 29.19 ($2CH_2$); 26.51 (CH_2); 24.83 ($2CH_2$); MS *m/z* molecular ion: 407.15 (cation), 159.00 (anion). IR (KBr, ν/cm^{-1}): 3164, 3112, 2942, 2889, 2865, 2143, 1564, 1463, 1169, 753, 623. Volatile content: 6%. Bromide content: 3 ppm.

1,8-Bis(3-methylimidazol-1-yl)octane Oxalate $[C_8(MIM)_2][C_0]$: $C_{18}H_{28}N_4O_4$; MW: 364.4393 g·mol^{-1}; white solid; 91%, T_g: -34 °C; ^{1}H NMR (600.13 MHz, D_2O): δ 8.68 (s, 2H, CH), 7.44 (t, J = 1.9 Hz, 2H, 2CH), 7.40 (t, J = 1.9 Hz, 2H, 2CH), 4.15 (t, J = 7.1 Hz, 4H, $2CH_2$), 3.86 (s, 6H, $2CH_3$), 1.83 (qui, J = 7.2 Hz, 4H, $2CH_2$), 1.34–1.22 (m, 8H, $4CH_2$)·^{13}C NMR (150.32 MHz, D_2O): δ 173.62 ($2COO^-$); 136.04 (2CH); 123.71 (2CH); 122.39 (2CH); 49.73 ($2CH_2$); 35.85 ($2CH_3$); 29.37 ($2CH_2$); 28.07 ($2CH_2$); 25.43 (2CH); MS *m/z* molecular ion: 365.30 (cation), 89.00 (anion). IR (KBr, ν/cm^{-1}): 3147, 3076, 2934, 2857, 2051, 1570, 1466, 1312, 1168, 729, 622. Volatile content: 9%. Bromide content: 13 ppm.

1,8-Bis(3-methylimidazol-1-yl)octane Malonate $[C_8(MIM)_2][C_1]$: $C_{19}H_{30}N_4O_4$; MW: 378.4659 g·mol^{-1}; white solid; 93%, T_g: −8.48 °C; ^{1}H NMR (600.13 MHz, D_2O): δ 9.58–9.55 (m, 2H, 2CH); 7.84 (s, 2H, 2CH); 7.76 (s, 2H, 2CH); 4.20 (t, J = 7 Hz, 4H, $2CH_2$); 3.89 (s, 6H, $2CH_3$); 2.72 (s, 2H, CH_2); 1.78 (qui, J = 7 Hz, 4H, $2CH_2$); 1.27–1.22 (m, 8H, $4CH_2$); ^{13}C NMR (150.32 MHz, $DMSO_{d6}$): δ 172.07 ($2COO^-$); 137.12 (2CH); 123.52 (2CH); 122.19 (2CH); 48.61 ($2CH_2$); 41.07 (CH_2); 35.66 ($2CH_3$); 29.32 ($2CH_2$); 28.03 ($2CH_2$); 25.29 ($2CH_2$); MS *m/z* molecular ion: 379.40 (cation), 103.00 (anion). IR (KBr, ν/cm^{-1}): 3093, 3069, 2052, 1573, 1467, 1356, 1166, 621, 545. Volatile content: 7%. Bromide content: 21 ppm.

1,8-Bis(3-methylimidazol-1-yl)octane Succinate $[C_8(MIM)_2][C_2]$: $C_{20}H_{32}N_4O_4$; MW: 392.4925 g·mol^{-1}; white solid; 90%, T_g: 8.56 °C; ^{1}H NMR (600.13 MHz, D_2O): δ 8.68 (s, 2H, 2CH); 7.43 (s, 2H, 2CH); 7.39 (s, 2H, 2CH); 4.13 (t, J = 7 Hz, 4H, $2CH_2$); 3.84 (s, 6H, $2CH_3$); 2.34 (s, 4H, $2CH_2$); 1.80 (qui, J = 7 Hz, 4H, $2CH_2$); 1.26–1.21 (m, 8H, $4CH_2$); ^{13}C NMR (150.32 MHz, $DMSO_{d6}$): δ 177.46 ($2COO^-$); 137.42 (2CH); 123.63 (2CH); 122.33 (2CH); 48.76 ($2CH_2$); 35.82 ($2CH_2$); 35.75 ($2CH_3$); 29.49 ($2CH_2$); 28.15 ($2CH_2$); 25.40 ($2CH_2$); MS *m/z* molecular ion: 393.40 (cation), 117.00 (anion). IR (KBr, ν/cm^{-1}): 3151, 3099, 2934, 2859, 1569, 1462, 1168, 758, 622. Volatile content: 10%. Bromide content: 5 ppm.

1,8-Bis(3-methylimidazol-1-yl)octane glutarate $[C_8(MIM)_2][C_3]$: $C_{21}H_{34}N_4O_4$; MW: 406.5191 g·mol^{-1}; pale yellow oil; 92%, T_{g1}: -31,46 °C, T_{g2}: 2.08 °C; ^{1}H NMR (600,13 MHz, D_2O): δ 8.68 (s, 2H, 2CH), 7.45 (t, J = 2 Hz, 2H, 2CH), 7.41 (t, J = 2 Hz, 2H, 2CH), 4.16 (t, J = 7 Hz, 4H, $2CH_2$), 3.87 (s, 6H, $2CH_3$), 2.18–2.16 (m, 4H, $2CH_2$), 1.83 (qui, J = 7 Hz, 4H, $2CH_2$), 1.79–1.74 (m, 2H, CH_2), 1.31–1.24 (m, 8H, $4CH_2$). ^{13}C NMR (150.32 MHz, $DMSO_{d6}$): δ 177.02 ($2COO^-$); 137.49 (2CH); 123.62 (2CH); 122.33 (2CH); 48.70 ($2CH_2$); 38.72 ($2CH_2$); 35.69 ($2CH_3$); 29.47 ($2CH_2$); 28.14 ($2CH_2$); 25.38 ($2CH_2$); 23.74 (CH_2). MS *m/z* molecular ion: 407.40 (cation), 131.10 (anion). IR (KBr, ν/cm^{-1}): 3237, 3148, 3092, 3069, 2961, 2938, 2920, 2857, 2052, 1570, 1467, 1399, 1166, 842, 774, 622, 545. Volatile content: 8%. Bromide content: 4 ppm.

1,8-Bis(3-methylimidazol-1-yl)octane adipate $[C_8(MIM)_2][C_4]$: $C_{22}H_{36}N_4O_4$; MW: 420.5456 g·mol^{-1}; pale yellow oil; 91%, T_g: −5.74 °C; ^{1}H NMR (600.13 MHz, $DMSO_{d6}$): δ 9.66 (s, 2H, 2CH); 7.84 (s, 2H, 2CH); 7.75 (s, 2H, 2CH); 4.18 (t, J = 7.141 Hz, 4H, $2CH_2$); 3.88 (s, 6H, $2CH_3$); 1.94–1.92 (m, 4H, $2CH_2$); 1.77 (qui, J = 7.216 Hz, 4H, $2CH_2$); 1.40–1.38 (m, 4H, $2CH_2$); 1.27–1.21 (m, 8H, $4CH_2$); ^{13}C NMR (150.32 MHz, $DMSO_{d6}$): δ 176.08 ($2COO^-$); 137.19 (2CH); 123.52 (2CH); 122.25 (2CH); 48.62 ($2CH_2$); 37.42 ($2CH_2$); 35.65 ($2CH_3$); 29.36 ($2CH_2$); 28.12 ($2CH_2$); 26.23 ($2CH_2$); 25.37 ($2CH_2$); MS *m/z* molecular ion: 421.60 (cation), 145.10 (anion). IR (KBr, ν/cm^{-1}): 3147, 3092, 3069, 2938, 2923, 2859, 2052, 1570, 1465, 1166, 842, 774, 621, 545. Volatile content: 9%. Bromide content: 16 ppm.

1,8-Bis(3-methylimidazol-1-yl)octane pimelate $[C_8(MIM)_2][C_5]$: $C_{23}H_{38}N_4O_4$; MW: 434.5722 g·mol^{-1}; pale yellow oil; 85%, T_g: -14.45 °C; ^{1}H NMR (600.13 MHz, D_2O): δ 8.69 (s, 2H, 2CH); 7.45–7.45 (m, 2H, 2CH); 7.41–7.41 (m, 2H, 2CH); 4.15 (t, J = 7.1 Hz, 4H, $2CH_2$); 3.86 (s, 6H, $2CH_3$); 2.13 (t, J = 7.6 Hz, 4H, $2CH_2$); 1.83 (qui, J = 7.12 Hz, 4H, $2CH_2$); 1.51 (qui, J = 7.6 Hz, 4H, $2CH_2$); 1.30–1.22 (m, 10H, $5CH_2$); ^{13}C NMR (150.32 MHz, $DMSO_{d6}$): δ 175.98 ($2COO^-$); 137.76 (2CH); 123.45 (2CH); 122.25 (2CH); 48.56 ($2CH_2$); 38.92 ($2CH_2$); 35.57 ($2CH_3$); 30.14 ($2CH_2$); 29.40 ($2CH_2$); 28.16 ($2CH_2$); 26,83 (CH_2); 25,40 ($2CH_2$). MS *m/z* molecular ion: 435.40 (cation), 159.10 (anion). IR (KBr, ν/cm^{-1}): 3148, 3092, 3068, 2939, 2921, 2857, 2052, 1570, 1466, 1166, 842, 774, 622, 545. Volatile content: 15%. Bromide content: 1 ppm.

1,10-Bis(3-methylimidazol-1-yl)decane Oxalate $[C_{10}(MIM)_2][C_0]$: $C_{20}H_{32}N_4O_4$; MW: 392.4925 g·mol^{-1}; white solid; 96%, T_g: −12.12 °C; ^{1}H NMR (600.13 MHz, D_2O): δ 8.69 (s, 2H, 2CH); 7.45 (s, 2H, 2CH); 7.40 (s, 2H, 2CH); 4.15 (t, J = 7.1 Hz, 4H, $2CH_2$); 3.86 (s, 6H, $2CH_3$); 1.82 (qui, J = 6.9 Hz, 4H, $2CH_2$); 1.26–1.21 (m, 12H, $6CH_2$); ^{13}C NMR (150.32 MHz, $DMSO_{d6}$): δ 163.99 ($2COO^-$); 136.55 (2CH); 123.56 (2CH); 122.25 (2CH); 48.73 ($2CH_2$); 35.76 ($2CH_3$); 29.41 ($2CH_2$); 28.71 ($2CH_2$); 28.33 ($2CH_2$); 25.47 ($2CH_2$). MS *m/z* molecular ion: 393.20 (cation), 89.10 (anion). IR (KBr, ν/cm^{-1}): 3149, 3094, 2929, 2855, 1570, 1463, 1168, 724, 622. Volatile content: 4%. Bromide content: 2 ppm.

1,10-Bis(3-methylimidazol-1-yl)decane Malonate $[C_{10}(MIM)_2][C_1]$: $C_{21}H_{34}N_4O_4$; MW: 406.5191 g·mol^{-1}; white solid; 98%, T_g: -12.0 °C; ^{1}H NMR (600.13 MHz, D_2O): δ 8.70 (s, 2H, 2CH); 7.46–7.45 (m, 2H, 2CH); 7.42–7.41 (m, 2H, 2CH); 4.15 (t, J = 7.1 Hz, 4H, $2CH_2$); 3.87 (s, 4H, $2CH_2$); 1.82 (qui, J = 7.1 Hz, 4H, $2CH_2$); 1.25–1.19 (m, 12H, $6CH_2$); ^{13}C NMR (150.32 MHz, $DMSO_{d6}$): δ 171.65 ($2COO^-$); 136.69 (2CH); 123.58 (2CH); 122.25 (2CH); 48.73 ($2CH_2$); 38.82 (CH_2); 35.71 ($2CH_3$); 29.40 ($2CH_2$); 28.72 ($2CH_2$); 28.34 ($2CH_2$); 25.49 ($2CH_2$). MS *m/z* molecular ion: 407.40 (cation), 103.10 (anion). IR (KBr, ν/cm^{-1}): 3149, 3093, 2930, 2856, 2073, 1572, 1462, 1356, 1168, 760, 621. Volatile content: 2%. Bromide content: 18 ppm.

1,10-Bis(3-methylimidazol-1-yl)decane succinate $[C_{10}(MIM)_2][C_2]$: $C_{22}H_{36}N_4O_4$; MW: 420.5456 g·mol^{-1}; pale yellow oil; 93%. T_g: 3.22 °C; ^{1}H NMR (600.13 MHz, D_2O): δ 8.69 (s, 2H, 2CH); 7.45–7.44 (m, 2H, 2CH); 7.41–7.40 (m, 2H, 2CH); 4.15 (t, J = 7.1 Hz, 4H, $2CH_2$); 3.86 (s, 6H, $2CH_3$); 2.39 (s, 4H, $2CH_2$); 1.84–1.79 (qui, J = 7.1 Hz, 4H, $2CH_2$); 1.28–1.20 (m, 12H, $6CH_2$); ^{13}C NMR (150.32 MHz, $DMSO_{d6}$): δ 176.62 ($2COO^-$); 137.80 (2CH); 123.49 (2CH); 122.24 (2CH); 48.57 ($2CH_2$); 35.55 ($2CH_3$); 29.45 ($4CH_2$); 28.61 ($2CH_2$); 28.25 ($2CH_2$); 25.43 ($2CH_2$). MS *m/z* molecular ion: 421.50 (cation), 117.00 (anion). IR (KBr, ν/cm^{-1}): 3421, 3100, 2934, 2856, 1640, 1569, 1463, 1414, 1169, 1110, 877, 759, 653, 623, 548. Volatile content: 7%. Bromide content: 10 ppm.

1,10-Bis(3-methylimidazol-1-yl)decane glutarate $[C_{10}(MIM)_2][C_3]$: $C_{23}H_{38}N_4O_4$; MW: 434.5722 g·mol^{-1}; pale yellow oil; 92%, T_g: −5.81 °C; ^{1}H NMR (600.13 MHz, D_2O): δ 8.70 (s, 2H, 2CH); 7.46 (s, 2H, 2CH); 7.42 (s, 2H, 2CH); 4.18–4.16 (m, 4H, $2CH_2$); 3.88 (s, 6H, $2CH_3$); 2.23–2.21 (m, 4H, $2CH_2$); 1.86–1.77 (m, 4H, $3CH_2$); 1.28–1.24 (m, 12H, $6CH_2$); ^{13}C NMR (150.32 MHz, $DMSO_{d6}$): δ 176.57 ($2COO^-$); 137.22 (2CH); 123.62 (2CH); 122.31 (2CH); 48.79 ($2CH_2$); 37.69 ($2CH_2$); 35.74 ($2CH_3$); 29.53 ($2CH_2$); 28.75 ($2CH_2$); 28.39 ($2CH_2$); 25.55 ($2CH_2$); 22.99 (CH_2). MS *m/z* molecular ion: 435.40 (cation), 131.10 (anion). IR (KBr, ν/cm^{-1}): 3151, 3100, 2962, 2929, 2856, 1568, 1449, 1398, 1168, 888, 742, 623. Volatile content: 8%. Bromide content: 4 ppm.

1,10-Bis(3-methylimidazol-1-yl)decane Adipate $[C_{10}(MIM)_2][C_4]$: $C_{24}H_{40}N_4O_4$; MW: 448.5988 g·mol^{-1}; colorless oil; 96%. T_g: -1.65 °C; ^{1}H NMR (600.13 MHz, D_2O): δ 8.70 (s, 2H, 2CH); 7.44 (m, 2H, 2CH); 7.40 (m, 2H, 2CH); 4.13 (t, J = 7.1 Hz, 4H, $2CH_2$); 3.84 (s, 6H, $2CH_3$); 2.12–2.10 (m, 4H, $2CH_2$); 1.81–1.76 (m, 4H, $2CH_2$); 1.47–1.45 (m, 4H, $2CH_2$); 1.22–1.17 (m, 12H, $6CH_2$); ^{13}C NMR (150.32 MHz, $DMSO_{d6}$): δ 176.73 ($2COO^-$); 137.18 (2CH); 123.63 (2CH); 122.32 (2CH); 48.83 ($2CH_2$); 38.24 ($2CH_2$); 35.77 ($2CH_3$); 29.56 ($2CH_2$); 28.82 ($2CH_2$); 28.45 ($2CH_2$); 26.71 ($2CH_2$); 25.59 ($2CH_2$). MS *m/z* molecular ion:

449.50 (cation), 145.00 (anion). IR (KBr, ν/cm^{-1}): 3148, 3092, 2930, 2857, 1571, 1460, 1403, 1168, 910, 736, 623, 509. Volatile content: 4%. Bromide content: 8 ppm.

1,10-Bis(3-methylimidazol-1-yl)decane pimelate [C_{10}(MIM)$_2$][C_5]: $C_{25}H_{42}N_4O_4$; MW: 462.6254 g·mol^{-1}; pale yellow oil; 90%, T_g: −0.28 °C; ^{1}H NMR (600.13 MHz, D_2O): δ 8.69 (s, 2H, 2CH); 7.45 (s, 2H, 2CH); 7.41 (s, 2H, 2CH); 4.16 (t, J = 7.1 Hz, 4H, 2CH$_2$); 3.87 (s, 6H, 2CH$_3$); 2.15 (t, J = 7.5 Hz, 4H, 2CH$_2$); 1.83 (qui, J = 7.1 Hz, 4H, 2CH$_2$); 1.54–1.49 (m, 4H, 2CH$_2$); 1.29–1.23 (s, 14H, 7CH$_2$); ^{13}C NMR (150.32 MHz, DMSO$_{d6}$): δ 176.93 (2COO$^-$); 137.34 (2CH); 123.63 (2CH); 122.34 (2CH); 48.81 (2CH$_2$); 38.69 (2CH$_2$); 35.74 (2CH$_3$); 30.11 (2CH$_2$); 29.60 (4CH$_2$); 28.85 (2CH$_2$); 28.48 (2CH$_2$); 26.70 (2CH$_2$); 25.61 (2CH$_2$). MS m/z molecular ion: 463.60 (cation), 159.00 (anion). IR (KBr, ν/cm^{-1}): 3452, 2932, 2858, 1640, 1564, 1463, 1403, 1169, 1087, 835, 757, 653, 623. Volatile content: 10%. Bromide content: 2 ppm.

3. Results and discussion

Twenty-four imidazole-based dicarboxylate ILs (18 new ones) were synthesized using the procedure proposed by Fukumoto et al. [26], which is based on an acid-base neutralization reaction. The structures and acronyms of the ILs used in this paper are shown in Table 1. This method proved to be effective for the synthesis of the desired ILs, leading to yields of 80–97%. The majority of the volatility observed in the ILs was from water and their amount ranged in 2–20% (w/w). The residual bromide in the compounds was determined — it was found that there was 1–62 ppm of bromide. The ILs with a dication spacer with four methylenes were solids, except the IL with malonate, which was isolated as an oil. On the other hand, when considering the ILs containing alkyl spacers with six and eight methylenes, half of the ILs were solids and the other half were oils. For ILs derived from dications with an alkyl spacer containing 10 methylenes, only the ILs with oxalate and malonate were solids — with the increase in methylene spacers in the anions, the ILs changed to oils. The results are shown in Table 1.

The structures of the ILs were confirmed by ^{1}H and ^{13}C NMR (see Figs. S1–S49), mass spectrometry (see Figs. S50–S97), and infrared spectroscopy (see Figs. S98–S121) — data are shown in the ESI. The ^{1}H and ^{13}C NMR spectra of all the ILs indicated chemical shift variation of the signal of methylene and carboxyl groups. Methylene signals of the IL were in a region of lower chemical shift (about 0.20 ppm) relative to the acid. The same trend was observed in the methylene signals from the middle of the chain that was in a region of lower chemical shift (0.10 ppm) in the ILs. Comparing the ^{13}C spectra of acid and respective IL, the carbonyl signal of acid moved two ppm to a region of major chemical shift when the IL was formed (carboxylate anion). Methylenes followed the same behavior, moving 2 ppm and 10 ppm higher in chemical shift when the IL was formed (See ^{1}H NMR Spectrum, Fig. S49, in the ESI). The electrospray ionization coupled to mass spectrometry (ESI-MS) was recorded for all ILs in positive and negative modes. For the positive mode, the monitored mass corresponded to a species formed by a dication and a monoanion (HOOC(CH$_2$)mCOO$^-$); whereas in the negative mode, the monitored mass corresponded to just a monoanion (HOOC(CH$_2$)mCOO$^-$). In the positive mode, it was also possible to identify the mass related to the interaction of one dication and one monoanion, which confirmed the presence of two species and the IL formation. The infrared spectra of the ILs had characteristic bands of the carboxylate and the imidazole ring and followed the same band pattern for all the ILs synthesized. The bands observed between 3100 and 2900 cm^{-1} are characteristic of symmetric and asymmetric axial deformation of CH in methylene groups as well as axial deformation of aromatic CH. Most important, the deprotonation of the carboxylic acid when the ILs formed was confirmed by the shift in the band corresponding to the axial deformation of the carbonyl, from 1681 cm^{-1} in the acid to 1575 cm^{-1} in the IL. In deprotonation, the C═O band moves in order to decrease the energy, because its vibrational mode is coupled to the other oxygen, thus giving rise to the asymmetric characteristic. Likewise, the C-O-H band changes to a higher energy when protonated, thus producing a COO$^-$ symmetric mode [40,41]. The disappearance of the characteristic band of the acid ($^-$OH) at the frequency of 3427 cm^{-1} can be seen when compared with the IR of the IL. In the IL, this band disappears and a band at 3341 appears at a much lower intensity, which can be attributed to both the presence of residual water and the vibrations from the NC(H)NCH [42]. The bands derived from the dication can also be seen in the regions between 1170 and 1150 cm^{-1}, where a symmetrical axial deformation band of the CH$_2$(N) and H$_3$C(N)CN ring is present — the band in the 790–750 cm^{-1} region with respect to the symmetrical angular

Table 1
Yield, volatile content, and physical appearance of the ILs.

IL	Yield (%)	Volatile content (%)[a]	Bromine content (ppm)	Physical appearance
[C_4(MIM)$_2$][C_0]	89	11	16	Pale yellow solid
[C_4(MIM)$_2$][C_1]	80	20	16	Viscous pale yellow
[C_4(MIM)$_2$][C_2]	94	6	43	White solid
[C_4(MIM)$_2$][C_3]	92	8	11	Pale yellow solid
[C_4(MIM)$_2$][C_4]	93	7	2	Pale yellow solid
[C_4(MIM)$_2$][C_5]	92	8	62	White solid
[C_6(MIM)$_2$][C_0]	97	0	20	White solid
[C_6(MIM)$_2$][C_1]	81	19	2	Pale yellow oil
[C_6(MIM)$_2$][C_2]	87	13	17	White solid
[C_6(MIM)$_2$][C_3]	91	9	18	Pale yellow oil
[C_6(MIM)$_2$][C_4]	82	18	14	Pale yellow oil
[C_6(MIM)$_2$][C_5]	94	6	3	Pale yellow solid
[C_8(MIM)$_2$][C_0]	91	9	13	White solid
[C_8(MIM)$_2$][C_1]	93	7	21	White solid
[C_8(MIM)$_2$][C_2]	80	10	5	White solid
[C_8(MIM)$_2$][C_3]	92	8	4	Pale yellow oil
[C_8(MIM)$_2$][C_4]	91	9	16	Pale yellow oil
[C_8(MIM)$_2$][C_5]	85	15	1	Pale yellow oil
[C_{10}(MIM)$_2$][C_0]	96	4	2	White solid
[C_{10}(MIM)$_2$][C_1]	92	2	18	White solid
[C_{10}(MIM)$_2$][C_2]	97	7	10	Pale yellow oil
[C_{10}(MIM)$_2$][C_3]	92	8	4	Pale yellow oil
[C_{10}(MIM)$_2$][C_4]	96	4	8	Colorless oil
[C_{10}(MIM)$_2$][C_5]	90	10	2	Pale yellow oil

[a]Volatile content determined by TGA.

deformation in the HCCH plane (imidazole ring) and an absorption band in the 640–620 cm^{-1} region refer to the symmetrical angular deformation outside the $H_3C(N)CN$ plane [43,44]. (See FTIR Spectrum, Fig. S121 in the ESI).

3.1. Thermal stability

The thermal properties of the ILs were determined using TGA (Figs. S122–S169 in the ESI) and DSC (Figs. S170–S193 in the ESI). The TGA was performed first and it indicated that thermal decomposition of the ILs occurred in multiple stages, except for $[C_4(MIM)_2][C_4]$, which lost nearly all its weight in one step. Considering the water content and residual volatiles observed in TGA curves and that the presence of water can alter the thermal behavior of ILs [45], the TGA was performed with an isotherm step (30 min at 120 °C) (Figs. S144-S191). The results showed that the residual water or other volatiles present in the ILs does not have an influence on their thermal decomposition. It is important to note that, for some ILs, total water elimination after the isotherm does not occur, even when performing isotherms for a slightly longer period (45–50 min). TGA curves are shown in the ESI. Thermal decomposition of ILs is reported in terms of $T_{d10\%}$ and T_{dmax} of the main decomposition step. The $T_{d10\%}$ and T_{dmax} for the main decomposition steps are shown in Table 2.

Considering the T_{dmax} of the first (main) step, for the whole IL series, the increase in the anion's alkyl chain led to an increase in the thermal stability from $[C_4(MIM)_2][C_0]$ until $[C_4(MIM)_2][C_3]$. The increase of the alkyl chain for $[C_4(MIM)_2][C_4]$ and $[C_4(MIM)_2][C_5]$ did not increase the stability of the IL. The decomposition temperature of the ILs with cations — $[C_6(MIM)_2]$ and $[C_8(MIM)_2]$ — increased with the increase in the methylene groups from oxalate to the glutarate anion, and then decreased for the adipate anion, but increased again for the pimelate anion. The decomposition temperature of the ILs with spacers with $n = 10$ increased from the oxalate to the adipate anion but decreased for the pimelate anion. When considering the T_{dmax} of the ILs with spacers of $n = 4$–10, the greater the amount of methylene in the cations and the anions, the greater the T_d.

Comparing the T_{dmax} of the ILs synthetized here with their analogues with bromide anions, it could be seen that they are less stable. They are also less stable that their monocationic analogues with mono- and dicarboxylate anions [46,47]. The thermal stability of the dicarboxylate-based $[C_4(MIM)_2]$ ILs synthesized in this work is lower than the ILs with anions derived from acids such as H_2SO_4, CF_3SO_3H, CH_3SO_3H, and p-TSA [48]. This behavior — in which ILs derived from strong acids have higher thermal stability than ILs derived from weak acids like carboxylic acid derivatives — has already been reported in the literature [48]. When comparing the T_{dmax} of cholinium-based ILs derived from oxalate, malonate, succinate, and glutarate [49], the thermal stability of dicarboxylate ILs is higher, which is consistent with reports in the literature that imidazolium-based ILs are more stable than tetraalkylammonium derivatives [50]. The ILs with cations $[C_4(MIM)_2]$ and $[C_6(MIM)_2]$ and the malonate, succinate, and glutarate anions have already been described in Guglielmero et al. [24] The T_{dmax} reported here and in Guglielmero et al. [24] were obtained via the same methodology and are similar, differing mostly only in the initial temperature. It is well known that besides the structure of ILs, contaminants and experimental conditions can affect the thermal stabilities of ILs [50]. This fact may be attributable to the presence of residual water and halogen in the samples, but Guglielmero et al. [24] did not report these data in their study. The T_{dmax} obtained for the bromide dicationic ILs under the same conditions were 314 °C for $[C_4(MIM)_2][2Br]$ and 316 °C for $[C_6(MIM)_2][2Br]$, $[C_8(MIM)_2][2Br]$, and $[C_{10}(MIM)_2][2Br]$. Thus, we can conclude that the alkyl spacer of the cation did not affect the T_d of those ILs.

Dicarboxylate anions increased the thermal stability of dicationic ILs; however, there is not a clear effect of the increase of the alkyl spacer of the anion on the thermal stability of the ILs. This result can be explained by reports in the literature that show that anions play an important role in the thermal stability of ILs [51], and that, in general, the onset of the decomposition of carboxylate ILs begins with a decarboxylation process [52].

3.2. Phase change behavior

Modulated differential scanning calorimetry detected the glass transition temperature (T_g) for the majority of ILs indicating a homogenous system. Solid-liquid and liquid-solid transitions were detected for eight ILs, which indicates that these ILs formed an amorphous and crystalline phase. The DSC curves of all ILs presented in this work can be accessed in the Supporting Information. The T_g values obtained by DSC measurement are shown in Table 3, and the $T_{S\text{-}L}$, $T_{L\text{-}S}$ and the enthalpy of fusion ($\Delta H_{S\text{-}L}$) and crystallization ($\Delta H_{L\text{-}S}$) values are shown in Table 4. T_g is a thermal parameter that can provide information about the cohesive energies of ILs. Low T_g values are generally associated with low cohesive energies in ILs [48]. In general, dicarboxylate ILs with $[C_4(MIM)_2]$ had lower T_g values when associated with an even number of carbon anions; while dicarboxylate ILs with $[C_6(MIM)_2]$, $[C_8(MIM)_2]$, and $[C_{10}(MIM)_2]$ had lower T_g values when associated with an odd number of carbon anions. With the exception of the IL $[C_4(MIM)_2][C_0]$, all ILs with the oxalate anion had the lowest T_g value in their series, which may indicate that the cohesive energy of these cations with this anion is low.

Some ILs presented a T_g and melting point, which indicates that there is a percentage of amorphous and crystalline material in their structures. In general, two types of behavior were observed for the dianionic-dicationic ILs studied via DSC. The first group of ILs had only

Table 2
Thermogravimetric analysis of the dicarboxylate-based ILs.

IL	$T^a_{d10\%}$	T^b_{d1}	T^c_{d2}	IL	$T^a_{d10\%}$	T^b_{d1}	T^c_{d2}
$[C_4(MIM)_2][C_0]$	230	242	290	$[C_8(MIM)_2][C_0]$	226	238	282
$[C_4(MIM)_2][C_1]$	207	247	279	$[C_8(MIM)_2][C_1]$	218	246	323
$[C_4(MIM)_2][C_2]$	235	254	328	$[C_8(MIM)_2][C_2]$	234	246	342
$[C_4(MIM)_2][C_3]$	249	264	345	$[C_8(MIM)_2][C_3]$	239	245	283
$[C_4(MIM)_2][C_4]$	231	264	–	$[C_8(MIM)_2][C_4]$	240	259	327
$[C_4(MIM)_2][C_5]$	244	264	296	$[C_8(MIM)_2][C_5]$	238	265	330
$[C_6(MIM)_2][C_0]$	228	243	299	$[C_{10}(MIM)_2][C_0]$	223	235	314
$[C_6(MIM)_2][C_1]$	235	243	313	$[C_{10}(MIM)_2][C_1]$	218	243	276
$[C_6(MIM)_2][C_2]$	235	255	336	$[C_{10}(MIM)_2][C_2]$	236	253	334
$[C_6(MIM)_2][C_3]$	243	270	333	$[C_{10}(MIM)_2][C_3]$	239	270	335
$[C_6(MIM)_2][C_4]$	238	266	334	$[C_{10}(MIM)_2][C_4]$	237	255	279
$[C_6(MIM)_2][C_5]$	245	277	333	$[C_{10}(MIM)_2][C_5]$	232	245	283

[a]10% mass loss temperature, [b]Maximum temperature of the first stage decomposition, [c]Maximum temperature decomposition of the second stage.

Table 3
Glass transition for dicarboxylate ILs.

IL	Tg^a (±SD) (°C)	IL	Tg^a (±SD) (°C)
$[C_4(MIM)_2][C_0]$	−7.33 ± 0.16	$[C_8(MIM)_2][C_0]$	−34.00 ± 0.29
$[C_4(MIM)_2][C_1]$	−0.78 ± 0.18	$[C_8(MIM)_2][C_1]$	−8.48 ± 0.55
$[C_4(MIM)_2][C_2]$	−29.35 ± 0.51	$[C_8(MIM)_2][C_2]$	−7.73 ± 0.26
$[C_4(MIM)_2][C_3]$	2.47 ± 0.01	$[C_8(MIM)_2][C_3]$	−31.36 ± 0.80
$[C_4(MIM)_2][C_4]$	−27.40 ± 1.11	$[C_8(MIM)_2][C_4]$	−5.74 ± 0.83
$[C_4(MIM)_2][C_5]$	−13.34 ± 0.38	$[C_8(MIM)_2][C_5]$	−14.45 ± 1.16
$[C_6(MIM)_2][C_0]$	−29.45 ± 0.36	$[C_{10}(MIM)_2][C_0]$	−12.12 ± 0.08
$[C_6(MIM)_2][C_1]$	−9.36 ± 0.78	$[C_{10}(MIM)_2][C_1]$	−11.94 ± 0.12
$[C_6(MIM)_2][C_2]$	−1.02 ± 0.09	$[C_{10}(MIM)_2][C_2]$	3.22 ± 0.32
$[C_6(MIM)_2][C_3]$	−10.78 ± 1.76	$[C_{10}(MIM)_2][C_3]$	–[b]
$[C_6(MIM)_2][C_4]$	−7.06 ± 0.21	$[C_{10}(MIM)_2][C_4]$	−1.65 ± 0.14
$[C_6(MIM)_2][C_5]$	−18.19 ± 0.31	$[C_{10}(MIM)_2][C_5]$	0.70 ± 0.36

[a]Values obtained by averaging two cycles. [b]These ILs had the following T_g values for the three different cycles: −13.9 °C (cycle 1), −5.88 °C (cycle 2), and −2.83 °C (cycle 3).

Table 4
$T_{S\text{-}L}$, $\Delta H_{S\text{-}L}$, $T_{L\text{-}S}$, and $\Delta H_{L\text{-}S}$ values for the ILs studied.

IL	$T_{S\text{-}L}$ (°C) (±SD)[a]	$\Delta H_{S\text{-}L}$ (kJ mol^{-1}) (±SD)	$T_{L\text{-}S}$ (°C) (±SD)[a]	$\Delta H_{L\text{-}S}$ (kJ mol^{-1}) (±SD)
$[C_4(MIM)_2][C_0]$	121 ± 0.19	7 ± 3.50	86 ± 2.15	4.70 ± 3.33
$[C_6(MIM)_2][C_1]$	115 ± 0.31	4 ± 0.95	94[b]	3.01[b]
$[C_6(MIM)_2][C_4]$	107 ± 0.15	10 ± 1.88	82 ± 0.45	4.68 ± 2.18
$[C_6(MIM)_2][C_5]$	110 ± 0.50	39 ± 5.40	36 ± 1.51	26.78 ± 0.45
$[C_8(MIM)_2][C_0]$	90 ± 1.44	4 ± 1.86	–[c]	–[c]
$[C_8(MIM)_2][C_2]$	162 ± 2.05	16 ± 5.77	104 ± 0.43	16.82 ± 1.15
$[C_{10}(MIM)_2][C_0]$	124 ± 0.05	10 ± 0.93	77 ± 0.45	10.00 ± 2.17
$[C_{10}(MIM)_2][C_5]$	119 ± 1.05	9 ± 6.11	82 [b]	6.97[b]

[a]Values obtained by averaging two cycles. [b]Crystallization only in the first cycle. [c]No crystallization.

a glass transition in the heating cycles, which indicates a totally amorphous material. This group included half of the ILs studied: $[C_4(MIM)_2][C_1]$, $[C_4(MIM)_2][C_3]$, $[C_4(MIM)_2][C_5]$, $[C_6(MIM)_2][C_2]$, $[C_6(MIM)_2][C_3]$, $[C_8(MIM)_2][C_1]$, $[C_8(MIM)_2][C_4]$, $[C_8(MIM)_2][C_5]$, $[C_{10}(MIM)_2][C_1]$, $[C_{10}(MIM)_2][C_2]$, $[C_{10}(MIM)_2][C_3]$, and $[C_{10}(MIM)_2][C_4]$, $[C_4(MIM)_2][C_2]$, $[C_4(MIM)_2][C_4]$, $[C_6(MIM)_2][C_0]$, and $[C_8(MIM)_2][C_3]$. The second behavior of the ILs indicated a glass transition, crystallization, and fusion. The presence of these thermal events indicates that the sample has a percentage of amorphous material and a crystalline percentage in its composition. The ILs in this group included the following: $[C_4(MIM)_2][C_0]$, $[C_6(MIM)_2][C_1]$, $[C_6(MIM)_2][C_4]$, $[C_6(MIM)_2][C_5]$, $[C_8(MIM)_2][C_0]$ $[C_8(MIM)_2][C_2]$, $[C_{10}(MIM)_2][C_0]$, and $[C_{10}(MIM)_2][C_5]$. With the exception of $[C_8(MIM)_2][C_0]$, all of these ILs also crystallize in the heating cycle.

The ILs with oxalate anions crystallized more readily, as can be seen by the melting of $[C_4(MIM)_2][C_0]$, $[C_8(MIM)_2][C_0]$, and $[C_{10}(MIM)_2][C_0]$. The melting point of these ILs was around 120 °C, except for $[C_8(MIM)_2][C_0]$ — in the first two cycles, besides a glass transition, it had a melting point; while in the third cycle, it had three vitreous transitions, which indicates the total amorphization of the sample after two heating–cooling cycles. These results show that the cation's spacer length has no effect on the melting point of these ILs. This trend is contrary to that found by Zhang et al. [12] for dicationic ILs with a bromine anion and a spacer length ranging from two to six methylenes. $[C_8(MIM)_2][C_1]$, $[C_8(MIM)_2][C_4]$, and $[C_8(MIM)_2][C_5]$ were crystalline, and had melting points between 107 and 115 °C, which indicates that there is no effect from the anion's spacer length on the melting point of these ILs. ILs with adipate and succinate anions are non-symmetrical and crystallized only with the cations $[C_6(MIM)_2]$ and $[C_8(MIM)_2]$, respectively. $[C_8(MIM)_2][C_2]$ had the highest melting point, which was unexpected, because, in general, symmetrical ILs are known to have higher melting points than non-symmetrical ILs [53,54]. It is likely that ionic, hydrogen-bond, and even dispersive interactions contribute more than molecular symmetry to the increase in the melting point of these ILs.

3.3. Heat of fusion analysis

The heat of fusion of the dicationic ILs, with a different chain spacer in the cations and anions, was obtained by integrating the peak area of the DSC peaks. The experimental results for the ILs which had melting points are shown in Table 4. In general, the change in the heat of fusion values was small — $[C_8(MIM)_2][C_0]$ and $[C_6(MIM)_2][C_1]$ had the lowest heat of fusion values (4 kJ mol^{-1}), which is probably because they have the highest amorphous content. $[C_6(MIM)_2][C_5]$ had the highest heat of fusion value (39 kJ mol^{-1}), which indicates great potential for use in thermal storage. A trend in which the heat of fusion of the ILs increases with the increase of the spacer chain length of the dication was observed. This trend is contrary to that found by Zhang et al. [12], who studied dicationic ILs with spacer lengths of 2–6 methylenes. These authors believed that this is because the spacer chain is a small fraction of the molecule compared to the greater imidazole moiety. Thus, here we can assume that the spacer chain of the dicationic ILs is a large fraction of the molecule compared to the imidazole moiety. The same tendency is observed for the spacer length of anions, in which the heat of fusion of ILs with $[C_6(MIM)_2]$ increases with the increase in the dianion's spacer chain length. If we look at the IL $[C_6(MIM)_2]$ with $[C_1]$, $[C_4]$, and $[C_5]$ anions, the increase in the heat of fusion value is small from $[C_1]$ to $[C_4]$ (about 6 kJ mol^{-1}); however, it is large from $[C_4]$ to $[C_5]$ (about 29 kJ mol^{-1}). Two asymmetric succinate and adipate anions were used in this work. As shown in Table 4, only two ILs crystallized with these anions: $[C_6(MIM)_2][C_4]$ and $[C_8(MIM)_2][C_2]$, which had small heat of fusion values (about 10 kJ mol^{-1}). This result shows that the asymmetric dianion spacer has no effect on the heat of fusion of ILs. It is likely that ionic and electrostatic interactions play a vital role in the heat of fusion. Another hypothesis to be investigated in the future is that the supramolecular arrangement favors the cation and anion interaction, and this factor contributes more than the molecular weight or the spacer length to the increase in the heat of fusion. In order to increase the crystallinity of the sample and improve the possibility of getting different polymorphic phases, which is often observed for ILs, DSC experiments of $[C_6(MIM)_2][C_5]$ with varying heating rate and an experiment with an annealing isotherm was performed. Results are given in Table S1 and S2 (in the ESI). The first set of experiments by (varying heating) showed that the melting shifts by 2 °C (error of 1.81%) over a heating range of 1°–20 °C, confirming that the endothermic peak is a thru melt. A slight increase in melting enthalpy at increased heating rate is expected and occurs because the transition occurs over a wider range of temperature due to the internal thermal gradient. In that case, liquid phase change material may exist at higher temperatures than the melting temperature, resulting in some sensible heat being included in the latent heat measurement [55]. In other words, the increase of melting enthalpies with higher DSC heating rates is due to the instrument sensitivity and resolution. For smaller heating rates, the instrument's resolution is improved at the cost of its sensitivity [56]. In turn, the Tg increases with a heating rate increase, as expected. Supercooling was observed at heating rates of 2, 10 and 20 °C min^{-1} with freezing point (at 70, 61 and 64 °C respectively) lower than the melting temperature in the first cooling cycle. The freezing point was observed in the second cooling cycle at the same heating rates, however at lower temperature and enthalpy. The difference between freezing point and melting temperature can be 20-30 K, and in the case of the second cycle it can be up to 50 K indicating a slower crystallization rate after each heating/cooling cycle. At heating rates of 1 and 5 °C min^{-1}, a cold crystallization was observed, which prevented freezing. This fact was observed at higher heating rates to other ILs and we speculate that at higher heating rates there is not enough time for crystal formation [57]. Even though an annealing isotherm (heating) was introduced, new crystalline phases (polymorphic phases) were not detected. After the annealing isotherm, *supercooling* was detected at 80 °C and cold crystallization was suppressed. The melting point (110 °C) and enthalpy of fusion was unaltered (Table S1 in the ESI).

3.4. Heat capacity

The heat capacity as a function of temperature for a series of dianionic ILs with cations $[C_4(MIM)_2]$ and $[C_6(MIM)_2]$ was determined through differential scanning calorimetry (DSC). These ILs were chosen because of they showed absence of phase transitions in a specific range of temperature (based on DSC curves). Although DSC curves for $[C_4(MIM)_2]^{2+}$ were obtained for the heat capacities between 298.15 and 348.15 K, the data analyzed were only between 314.15 and 343.15 K, while for $[C_6(MIM)_2]$ the heat capacities were obtained between 298.15 and 323.15 K, and the data analyzed were only between 306.15 and 323.15 K, because the samples are not entirely thermally stable at the extreme temperatures of the aforementioned limits. Table 5 shows heat capacity values at different temperatures and

Table 5
Experimental heat capacities dicationic dianionic ILs and mono- and dicationic from literature.

IL	Cp ($J\ mol^{-1}\ K^{-1}$)	Cp ($J\ g^{-1}\ K^{-1}$)[a]	IL	Cp ($J\ g^{-1}\ K^{-1}$)[b,c]
$[C_4(MIM)_2][C_1]$	573	1.805	$[BisEt(MIM)_2][Br]$	2.82
$[C_4(MIM)_2][C_2]$	372	1.230	$[BisPr(MIM)_2][Br]$	2.85
$[C_4(MIM)_2][C_3]$	424	1.245	$[C_4(MIM)_2][Br]$	2.82
$[C_4(MIM)_2][C_4]$	461	1.346	$[BisPent(MIM)_2][Br]$	2.78
$[C_4(MIM)_2][C_5]$	623	1.674	$[C_6(MIM)_2][Br]$	2.80
$[C_6(MIM)_2][C_1]$	722	2.096	[EtMIM][Br]	1.08
$[C_6(MIM)_2][C_4]$	552	1.606	$[ButMIM][BF_4]$	1.12

[a]Determined at 323.5 K. [b]Determined at 333–453 K. [c]References [12,13].

Fig. 2 shows the temperature dependence of heat capacity for $[C_4(MIM)_2]$ and $[C_6(MIM)_2]$, respectively. The data obtained for ILs with $[C_4(MIM)_2]$ and $[C_6(MIM)_2]$ dicarboxylate anions showed an increase in heat capacity with increasing temperature. Thus trend is expected because heat capacity reflects the internal energy, which is influenced by the rotation and vibrational energy. As the temperature rises, more number of molecules reach energy levels to become excited and the internal energy increase, thus, the heat capacity also increases. Additionally, this trend is commonly observed for monocationic ILs [58,59]. The heat capacity values of each IL are given as an average of three measurements. For each heat capacity, at a given temperature, the data overlap with the standard deviation values (available in the ESI). The temperature dependence of heat capacity for $[C_4(MIM)_2]$ and $[C_6(MIM)_2]$ dicarboxylate anions are very well fitted by a quadratic polynomial function ($C_p = a + bT + cT^2$), with a squared correlation factor (R^2) close to 1 (data available in the ESI).

In the range of temperature studied, for the cation $[C_4(MIM)_2]$ the highest heat capacity follows the following order $[C_2] < [C_3] < [C_4] < [C_5] < [C_1]$. This result indicates that an increase in the molecular weight of the anion (addition of a $-CH_2$ group) promotes an increase in heat capacity, except $[C_4(MIM)_2][C_1]$, which had the second highest heat capacity despite having the smallest alkyl chain among the anions (Fig. 1). Another interesting result was observed with $[C_4(MIM)_2][C_2]$ and $[C_4(MIM)_2][C_4]$, which experienced the greatest increase in heat capacity with the increase in temperature. When we take into account ILs with the same anion (e.g., malonate or adipate), we can see that ILs with the $[C_6(MIM)_2]$ cation have greater heat capacity than those ILs with the $[C_4(MIM)_2]$ cation. It is important to note that the heat capacity of $[C_4(MIM)_2]$ ILs with malonate and pimelate is similar to $[C_6(MIM)_2]$ with malonate and adipate anions. These results can be explained by considering that heat capacity depends on the number of translation, vibration, and rotation energy storage modes in the molecule. Thus, it would be expected that molecules with more energy modes should have a higher heat capacity [13]. Unfortunately, there are few reports about the determination of the heat capacity of imidazolium-based dicationic ILs, and the available studies do not include organic anions. However, it is reported that dicationic ILs with bromine counterion have higher heat capacity than that of analogous monocationic ILs [12,13]. The dicationic ILs with bromine have a higher Cp value (about 2.8 $J\ g^{-1}\ K^{-1}$) than dicarboxylate dicationic ILs (the highest Cp value was 2.1 $J\ g^{-1}\ K^{-1}$). However, our results clearly show that the dicarboxylate anions have a strong effect on the heat capacity of dicationic ILs and it use in specific applications as thermal storage fluids can be justified considering that they can be less toxic and more environmentally friendly when compared to bromine anion. When comparing mono- and dicationic ILs, the authors [12,13] considered that the presence of additional hydrogen bonds — which offers more modes of vibration — is responsible for the higher Cp of the dicationic ILs. However, this cannot be a rule when the anions are not halogens. Organic anions could be adding more modes of vibration and, by this logic, they should have a higher Cp. One alternative explanation is that the greater ionic character of the hydrogen bonds with halogens (higher electronic density) favors the cation and anion interaction more than in the case of the carboxylate anion; thus, halogenated ILs might have higher Cp values.

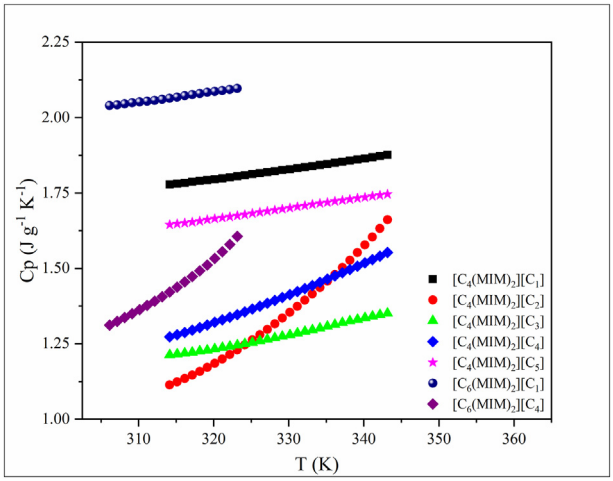

Fig. 2. Heat capacity as a function of temperature for all ILs studied.

3.5. Thermal storage density

The thermal storage density (Es) of the dicarboxylate dicationic ILs was determined aiming new possibilities for applications of ILs in many fields. The Es was calculated by Eq. (2) based on the density (ρ) and heat capacity of ILs.

$$Es = \rho C_p (T_{out} - T_{in}) \quad (2)$$

To confirm the accuracy of our experimental measurements, the density and heat capacity was determined using computational simulations (Table 6). Therefore, Es was determined using experimental and simulated data of four ILs which were selected to allow the evaluation of anion and cation effects in the thermal storage density values. In the determination of Es a temperature change ($T_{out} - T_{in}$) of 100 K was chosen because it is commonly used in solar energy applications to compare the difference in operating temperatures. [61,62] Results of Es are given in Table 6.

The results show that simulation and experimental densities and heat capacity results for ILs with smaller anions were similar (smaller % error), while for ILs with larger anions the % error was greater. The density for the ILs showed in Table 6 is similar to the density of monocationic ILs with inorganic anions such as NTf_2, BF_4 and NO_3 [25] and smaller than that for the dicationic imidazolium-

Table 6
Experimental and simulated ILs densities and molar heat capacity.

IL	Density (g cm^{-3}) (± SD)			Cp (J mol^{-1} K^{-1})		
	Simulation	Experimental	Error (%)	Simulation	Experimental	Error (%)
Water (TIP3P)	1.008	0.997[31]	−1.09	67.12	68.72[a]	2.34[a]
$[C_4(MIM)_2][A_1]$	1.24	1.33 ± 0.01	6.77	576.44	573.00	−0.60
$[C_4(MIM)_2][A_5]$	1.15	1.32 ± 0.06	12.87	675.48	623.00	−8.42
$[C_6(MIM)_2][A_1]$	1.20	1.29 ± 0.03	6.98	747.50	722.00	−3.53
$[C_6(MIM)_2][A_5]$	1.12	1.34 ± 0.15	16.42	846.38	[b]-	[b]-

[a]Considering Cp of water as 75 J mol^{-1} K^{-1} [31,60] the error is 10.5% [60]. [b]Cp was not obtained because there is not range of temperature without Cp variation in DSC traces.

based ILs with NTf_2, BF_4 and NO_3 [25]. The fact that the dicationic imidazolium-based ILs with NTf_2, BF_4 and NO_3 are liquid at 297 K can explain their higher density compared with dicationic imidazolium-based dicarboxylate ILs. The heat capacity of for the ILs shown in Table 6 is higher than for monocationic ILs [12,34]. However, it was smaller than dicationic ILs with the same dication and a bromine anion [34]. As expected, the Es determined using experimental data was overestimated compared with simulation, but the structural dependence of Es was the same. When ILs have a spacer with four and six methylenes, it is noted that the larger the anion, the smaller the Es. When comparing ILs with the same anion, ILs with a larger spacer showed higher Es. The Es values of ILs with dicarboxylate anions are higher than those of the monocationic ILs, but smaller than those of dicationic ILs with bromine anion Table 7. These results lead us to discard the hypothesis that organic anions would have a higher heat capacity than ILs analogues with bromine anion. On the other hand, they indicate that the greater ionic character of the hydrogen bonds of the cation with halogen anion (higher electronic density) favors the cation and anion interaction more than the carboxylate anion and result in higher heat capacity and Es values.

When the Es values of the dicarboxylate dicationic ILs are compared with conventional oils used for storage of thermal energy [63], such as mineral oil (Es = 200 MJ m^{-3}), synthetic oil (Es = 207 MJ m^{-3}) and silicone oil (Es = 189 MJ m^{-3}), we can see that Es values are higher than the Es of thermal oils. These results highlight the potential application of the dicationic dicarboxylate ionic liquids as a heat transfer fluid and thermal energy storage.

3.6. Solubility

The solubility of the dicarboxylated ILs was tested in 11 different solvents commonly found in research laboratories, with various polarities. The results, which are shown in Table 8 indicated good solubility of the ILs in polar protic solvents (water, methanol, and ethanol), but, surprisingly, they did not show the same behavior in isopropanol. The ILs derived from the $[C_8(MIM)_2]^{2+}$ and $[C_{10}(MIM)_2]^{2+}$ dications had average solubility in this solvent — only $[C_8(MIM)_2][C_2]$ had good solubility, while $[C_{10}(MIM)_2][C_0]$ was not soluble. Interestingly, for the dications $[C_4(MIM)_2]^{2+}$ and $[C_6(MIM)_2]^{2+}$, which have smaller spacer chains, only the ILs $[C_4(MIM)_2][C_4]$, $[C_6(MIM)_2][C_0]$, $[C_6(MIM)_2][C_2]$, and $[C_6(MIM)_2][A_3]$ had moderate solubility in isopropanol (0.1 g/3 mL). All the ILs were soluble in DMSO and had low solubility in the other aprotic polar solvents (acetonitrile, acetone, ethyl acetate, and chloroform), as well as in the apolar solvents (hexane and toluene). This behavior is directly related to the structure of the ILs. The presence of the carboxylate group in the anion facilitates solubilization in polar protic solvents, and it can be seen that the increase in the anion chain within the same series of compounds does not modify the solubility of the ILs. Hydroxyl-functionalized ammonium dicationic ILs containing aromatic carboxylate anions behave similarly to dicarboxylate ILs in the solvents studied [64]. The presence of hydroxyl-functionalized groups in the cation makes the solubility more similar to the dicarboxylate ILs synthesized in this work.

4. Conclusion

Thermal analysis of dicationic dicarboxylate ILs showed that most of these ILs undergo multiple decomposition steps and can be safely used at relatively high temperatures. The DSC analyses showed that there was no effect from the dianion spacer length on the melting point of these ILs. However, a trend in which the heat of fusion of the ILs increases with the increase in the dication spacer chain length was observed. The same tendency was observed for the spacer length of the dianions. Our results also showed that the anion has a strong effect on the heat capacity of dicationic ILs and that the ionic character of the hydrogen bonds of the cation and anion results in higher heat capacity and Es values. Furthermore, the dicationic dicarboxylate ILs have a higher heat capacity than monocationic ILs, but a smaller than analogous dicationic ILs with bromine. In terms of thermal storage, the dicationic dicarboxylate ILs have higher Es than thermal oils and $[C_6(MIM)_2][C_1]$ and $[C_6(MIM)_2][C_5]$ were the most promising ILs. Despite of the ILs showed smaller Es value than bromide analogues, it use in specific applications as thermal storage fluids can be justified when toxicity of bromine anion is a problem.

Author contributions

The manuscript was written with contributions from all authors. All authors have given approval to the final version of the manuscript.

Table 7
Thermal storage densities (MJ m^{-3}) values of dicationic dianionic ionic liquids and various mono- and dicationic ILs reported in the literature for a 100 K change.

IL	Simulation	Experimental	Error (%)	IL	Experimental
$[C_4(MIM)_2][C_1]$	221	240	8	$[C_4(MIM)_2][2Br]$	>423 [12]
$[C_4(MIM)_2][C_5]$	205	221	7	$[C_6(MIM)_2][2Br]$	>425[12]
$[C_6(MIM)_2][C_1]$	256	270	5	$[C_4MIM][BF_4]$	>200 [61]
$[C_6(MIM)_2][C_5]$	233	–[a]	–[a]	$[C_6MIM][PF_6]$	>210 [62]

[a]Heat capacity was not obtained because there is not range of temperature without heat capcity variation in DSC traces.

Table 8
Solubilities of ILs in molecular solvent.

IL	Water	Methanol	Ethanol	Isopropanol	DMSO	Acetonitrile	Acetone	Ethyl Acetate	Chloroform	Toluene	Hexane
$[C_4(MIM)_2][C_0]$	+	+	+	−	+	−	−	−	−	−	−
$[C_4(MIM)_2][C_1]$	+	+	+	−	+	−	−	−	−	−	−
$[C_4(MIM)_2][C_2]$	+	+	+	−	+	−	−	−	−	−	−
$[C_4(MIM)_2][C_3]$	+	+	+	−	+	−	−	−	−	−	−
$[C_4(MIM)_2][C_4]$	+	+	+	±	+	−	−	−	−	−	−
$[C_4(MIM)_2][C_5]$	+	+	+	−	+	−	−	−	−	−	−
$[C_6(MIM)_2][C_0]$	+	+	+	±	+	±	−	−	±	−	−
$[C_6(MIM)_2][C_1]$	+	+	+	−	+	−	−	−	−	−	−
$[C_6(MIM)_2][C_2]$	+	+	+	±	+	±	−	±	−	−	−
$[C_6(MIM)_2][C_3]$	+	+	+	±	+	−	−	−	−	−	−
$[C_6(MIM)_2][C_4]$	+	+	+	−	+	−	−	−	−	−	−
$[C_6(MIM)_2][C_5]$	+	+	+	−	+	−	−	−	−	−	−
$[C_8(MIM)_2][C_0]$	+	+	+	±	+	−	−	−	−	−	−
$[C_8(MIM)_2][C_1]$	+	+	+	±	+	−	−	−	−	−	−
$[C_8(MIM)_2][C_2]$	+	+	+	+	+	−	−	−	−	−	−
$[C_8(MIM)_2][C_3]$	+	+	+	±	+	−	−	−	−	−	−
$[C_8(MIM)_2][C_4]$	+	+	+	±	+	−	−	−	−	−	−
$[C_8(MIM)_2][C_5]$	+	+	+	±	+	−	−	−	−	−	−
$[C_{10}(MIM)_2][C_0]$	+	+	+	−	+	−	−	−	−	−	−
$[C_{10}(MIM)_2][C_1]$	+	+	+	±	+	−	−	−	−	−	−
$[C_{10}(MIM)_2][C_2]$	+	+	+	±	+	−	−	−	−	−	−
$[C_{10}(MIM)_2][C_3]$	+	+	+	±	+	−	−	−	−	−	−
$[C_{10}(MIM)_2][C_4]$	+	+	+	±	+	−	−	−	−	−	−
$[C_{10}(MIM)_2][C_5]$	+	+	+	±	+	−	−	−	−	−	−

[a] + = good solubility, ± = moderate solubility, and – = poor solubility.

CRediT authorship contribution statement

Bruna L. Kuhn: Investigation, Writing - review & editing.**Bárbara F. Osmari:**Investigation, Writing - review & editing.**Thaíse M. Heinen:**Investigation, Writing - review & editing.**Helio G. Bonacorso:**Investigation, Writing - review & editing.**Nilo Zanatta:**Investigation, Writing - review & editing.**Steven O. Nielsen:**Investigation, Writing - review & editing.**Dineli T.S. Ranathunga:**Investigation, Writing - review & editing.**Marcos A. Villetti:**Investigation, Writing - review & editing. **Clarissa P. Frizzo:**Investigation, Writing - review & editing.

Declaration of competing interest

Hereby, Clarissa Piccinin Frizzo author of the manuscript named Dicationic Imidazolium-Based Dicarboxylate Ionic Liquids: Thermophysical Properties and Solubility, declare that there is no personal, commercial, academic, political and financial conflict in this manuscript.

Acknowledgments

The authors are thankful for the financial support from: the National Council of Scientific and Technological Development (Conselho Nacional de Desenvolvimento Científico e Tecnológico — CNPq) — proc. no. 432201/2018-1); and the Rio Grande do Sul State Foundation for Research Support (Fundação de Amparo à Pesquisa do Estado do Rio Grande do Sul — FAPERGS) — grant no. 17/2551-0000944-4 and grant no. 16/2551-0000477-3. The fellowships from CNPq (grant no. 306389/2018-5 for C.P.F. and CAPES (for B.L.K.) are also acknowledged. This study was partly financed by the Coordination for the Improvement of Higher Education Personnel (Coordenação de Aperfeiçoamento de Pessoal de Nível Superior — CAPES) — Finance Code 001.

Appendix A. Supplementary data

The Supporting Information (NMR ^1H and ^{13}C, mass spectrum, IR spectrum, TGA thermograms, DSC curves, graphs and tables of individual heat capacity) is available free of charge. doi:https://doi.org/10.1016/j.molliq.2020.112983.

References

[1] M.A.P. Martins, C.P. Frizzo, A.Z. Tier, D.N. Moreira, N. Zanatta, H.G. Bonacorso, Update 1 of: ionic liquids in heterocyclic synthesis, Chem. Rev. 114 (2014) PR1–PR70, https://doi.org/10.1021/cr500106x.
[2] M.G. Montalbán, G. Víllora, P. Licence, Ecotoxicity assessment of dicationic versus monocationic ionic liquids as a more environmentally friendly alternative, Ecotoxicol. Environ. Saf. 150 (2018) 129–135, https://doi.org/10.1016/j.ecoenv.2017.11.073.
[3] A. Pinkert, K.N. Marsh, S. Pang, M.P. Staiger, Ionic liquids and their interaction with cellulose, Chem. Rev. 109 (2009) 6712–6728.
[4] P.A. Hunt, C.R. Ashworth, R.P. Matthews, Hydrogen bonding in ionic liquids, Chem. Soc. Rev. 44 (2015) 1257–1288, https://doi.org/10.1039/C4CS00278D.
[5] I.M. Gindri, D.A. Siddiqui, P. Bhardwaj, L.C. Rodriguez, K.L. Palmer, C.P. Frizzo, M.A.P. Martins, D.C. Rodrigues, Dicationic imidazolium-based ionic liquids: a new strategy for non-toxic and antimicrobial materials, RSC Adv. 4 (2014) 62594–62602, https://doi.org/10.1039/C4RA09906K.
[6] I.M. Gindri, D.A. Siddiqui, C. Davis, C.P. Frizzo, M.A.P. Martins, D.C. Rodrigues, Improvement of tribological and anti-corrosive performance of titanium surfaces using dicationic imidazolium-based ionic liquids coatings, ACSApplied Mater. Interfaces 6 (2016) 78795–78802, https://doi.org/10.1039/C6RA13961Bunder Rev.
[7] F. Pagano, C. Gabler, P. Zare, M. Mahrova, N. Dörr, R. Bayon, X. Fernandez, W. Binder, M. Hernaiz, E. Tojo, A. Igartua, Dicationic ionic liquids as lubricants, Proc. Inst. Mech. Eng. Part J J. Eng. Tribol. 226 (2012) 952–964, https://doi.org/10.1177/1350650112458873.
[8] X.W. Li, Y.A. Gao, J. Liu, L.Q. Zheng, B. Chen, L.Z. Wu, C.H. Tung, Aggregation behavior of a chiral long-chain ionic liquid in aqueous solution, J. Colloid Interface Sci. 343 (2010) 94–101, https://doi.org/10.1016/j.jcis.2009.11.010.
[9] M. Anouti, J. Jones, A. Boisset, J. Jacquemin, M. Caillon-Caravanier, D. Lemordant, Aggregation behavior in water of new imidazolium and pyrrolidinium alkycarboxylates protic ionic liquids, J. Colloid Interface Sci. 340 (2009) 104–111, https://doi.org/10.1016/j.jcis.2009.07.061.
[10] I.M. Gindri, D.A. Siddiqui, C.P. Frizzo, M.A.P. Martins, D.C. Rodrigues, Ionic liquid coatings for titanium surfaces: effect of IL structure on coating profile, ACS Appl. Mater. Interfaces 7 (2015) 27421–27431, https://doi.org/10.1021/acsami.5b09309.
[11] M.T. Zaky, M.I. Nessim, M.A. Deyab, Synthesis of new ionic liquids based on dicationic imidazolium and their anti-corrosion performances, J. Mol. Liq. 15 (2019), 111230. https://doi.org/10.1016/j.molliq.2019.111230.
[12] H. Zhang, W. Xu, J. Liu, M. Li, B. Yang, Thermophysical properties of dicationic imidazolium-based ionic compounds for thermal storage, J. Mol. Liq. 282 (2019) 474–483, https://doi.org/10.1016/j.molliq.2019.03.012.
[13] H. Zhang, J. Liu, M. Li, B. Yang, Functional groups in geminal imidazolium ionic compounds and their influence on thermo-physical properties, J. Mol. Liq. 269 (2018) 738–745, https://doi.org/10.1016/j.molliq.2018.08.037.

[14] X.J. Yang, P. Zhang, W. Lv, T. Zhou, P. Li, M. Zhao, Aggregation behavior of imidazolium-based amino acid ionic liquid surfactants in aqueous solution: the effect of amino acid counterions, J. Surfactant Deterg. (2019) https://doi.org/10.1002/jsde.12270.

[15] D.V. Kawadkar, S.P. Zodape, Thermophysical properties of dicationic ionic liquids under the influence of amino acid, J. Chem. Eng. Data 64 (2019) 421–432, https://doi.org/10.1021/acs.jced.8b00349.

[16] K. Ali, R. Moshikur, R. Wakabayashi, Y. Tahara, Synthesis and characterization of choline – fatty-acid-based ionic liquids: a new biocompatible surfactant, J. Colloid Interface Sci. 551 (2019) 72–80.

[17] C. Florindo, F.S. Oliveira, L.P.N. Rebelo, A.M. Fernandes, I.M. Marrucho, Insights into the synthesis and properties of deep eutectic solvents based on choline chloride and carboxylic acids, ACS Sustain. Chem. Eng. 2 (2014) 2416–2425, https://doi.org/10.1021/sc500439w.

[18] M. Niemczak, D.K. Kaczmarek, T. Klejdysz, D. Gwiazdowska, K. Marchwińska, J. Pernak, Ionic liquids derived from vitamin C as multifunctional active ingredients for sustainable stored-product management, ACS Sustain. Chem. Eng. 7 (2019) 1072–1084, https://doi.org/10.1021/acssuschemeng.8b04696.

[19] G.M.J. Al Kaisy, M.I. Abdul Mutalib, T.V.V.L.N. Rao, Novel halogen free hydrophobic trioctylammonium-based protic ionic liquids with carboxylate anions: synthesis, characterization, and thermophysical properties, J. Mol. Liq. 242 (2017) 349–356, https://doi.org/10.1016/j.molliq.2017.07.037.

[20] S. Baj, T. Krawczyk, A. Dabrowska, A. Siewniak, A. Sobolewski, Absorption of carbon dioxide in aqueous solutions of imidazolium ionic liquids with carboxylate anions, Korean J. Chem. Eng. 32 (2015) 2295–2299, https://doi.org/10.1007/s11814-015-0082-2.

[21] N. Bicak, A new ionic liquid: 2-hydroxy ethylammonium formate, J. Mol. Liq. 116 (2005) 15–18, https://doi.org/10.1016/j.molliq.2004.03.006.

[22] M.I. Hossain, M. El-Harbawi, Y.A. Noaman, M.A. Bustam, N.B.M. Alitheen, N.A. Affandi, G. Hefter, C.Y. Yin, Synthesis and anti-microbial activity of hydroxylammonium ionic liquids, Chemosphere 84 (2011) https://doi.org/10.1016/j.chemosphere.2011.02.048.

[23] M.A. Aboudzadeh, M.E. Muñoz, A. Santamaría, D. Mecerreyes, New supramolecular ionic networks based on citric acid and geminal dicationic ionic liquids, RSC Adv. 3 (2013) 8677, https://doi.org/10.1039/c3ra40629f.

[24] L. Guglielmero, A. Mezzetta, L. Guazzelli, C.S. Pomelli, F. D'Andrea, C. Chiappe, Systematic synthesis and properties evaluation of dicationic ionic liquids, and a glance into a potential new field, Front. Chem. 6 (2018) 1–16, https://doi.org/10.3389/fchem.2018.00612.

[25] H. Shirota, T. Mandai, H. Fukazawa, T. Kato, Comparison between dicationic and monocationic ionic liquids: liquid density, thermal properties, surface tension, and shear viscosity, J. Chem. Eng. Data 56 (2011) 2453–2459, https://doi.org/10.1021/je2000183.

[26] K. Fukumoto, M. Yoshizawa, H. Ohno, Room temperature ionic liquids from 20 natural amino acids, J. Am. Chem. Soc. 127 (2005) 2398–2399, https://doi.org/10.1021/ja043451i.

[27] N.S. Osborne, H.F. Stimson, D.C. Ginnings, Measurements of heat capacity and heat of vaporization of water in the range 0 to 100 °C, J. Res. Natl. Bur. Stand. 23 (1939) 197–260.

[28] L.F. Chiu, H.F. Liu, M.H. Li, Heat capacity of alkanolamines by differential scanning calorimetry, J. Chem. Eng. Data 44 (1999) 631–636, https://doi.org/10.1021/je980217x.

[29] J.C. Phillips, R. Braun, W. Wang, J. Gumbart, E. Tajkhorshid, E. Villa, C. Chipot, R.D. Skeel, L. Kalé, K. Schulten, Scalable molecular dynamics with NAMD, J. Comput. Chem. 26 (2005) 1781–1802, https://doi.org/10.1002/jcc.20289.

[30] A.S. Gross, A.T. Bell, J.W. Chu, Thermodynamics of cellulose solvation in water and the ionic liquid 1-butyl-3-methylimidazolim chloride, J. Phys. Chem. B 115 (2011) 13433–13440, https://doi.org/10.1021/jp202415v.

[31] K.G. Sprenger, V.W. Jaeger, J. Pfaendtner, The general AMBER force field (GAFF) can accurately predict thermodynamic and transport properties of many ionic liquids, J. Phys. Chem. B 119 (2015) 5882–5895, https://doi.org/10.1021/acs.jpcb.5b00689.

[32] T. Yan, C.J. Burnham, M.G. Del Pópolo, G.A. Voth, Molecular dynamics simulation of ionic liquids: the effect of electronic polarizability, J. Phys. Chem. B 108 (2004) 11877–11881, https://doi.org/10.1021/jp047619y.

[33] A.T. Nasrabadi, L.D. Gelb, Structural and transport properties of tertiary ammonium triflate ionic liquids: a molecular dynamics study, J. Phys. Chem. B 121 (2017) 1908–1921, https://doi.org/10.1021/acs.jpcb.6b12418.

[34] C.M. Tenney, M. Massel, J.M. Mayes, M. Sen, J.F. Brennecke, E.J. Maginn, A computational and experimental study of the heat transfer properties of nine different ionic liquids, J. Chem. Eng. Data 59 (2014) 391–399, https://doi.org/10.1021/je400858t.

[35] X. Zhong, Z. Liu, D. Cao, Improved classical united-atom force field for Imidazolium-based ionic liquids: tetrafluoroborate, hexafluorophosphate, methylsulfate, trifluoromethylsulfonate, acetate, trifluoroacetate, and bis(trifluoromethylsulfonyl) amide, J. Phys. Chem. B 115 (2011) 10027–10040.

[36] V.V. Chaban, I.V. Voroshylova, O.N. Kalugin, A new force field model for the simulation of transport properties of imidazolium-based ionic liquids, Phys. Chem. Chem. Phys. 13 (2011) 7910–7920, https://doi.org/10.1039/c0cp02778b.

[37] T.G.A. Youngs, C. Hardacre, Application of static charge transfer within an ionic-liquid force field and its effect on structure and dynamics, ChemPhysChem 9 (2008) 1548–1558, https://doi.org/10.1002/cphc.200800200.

[38] L. Martínez, R. Andrade, E.G. Birgin, J.M. Martínez, Packmol: a package for building initial configurations for molecular dynamics simulations, J. Comput. Chem. 30 (2008) 2157–2164, https://doi.org/10.1002/jcc.

[39] A.I. Vogel, A.R. Tatchell, B.S. Furniss, A.J. Hannaford, P.W.G. Smith, Vogel's Textbok of Practical Organic Chemistry, 5th ed. Pearson, 1996.

[40] B. Koleva, T. Kolev, M. Spiteller, Spectroscopic analysis and structural elucidation of small peptides – experimental and theoretical tools, in: J.C. Taylor (Ed.), Adv. Chem. Res, 3rd ed.Nova Science Publishers Inc, N.Y., US 2010, pp. 675–755.

[41] N.P.G. Roeges, A Guide to the Complete Interpretation of Infrared Spectral of Organic Structures, 1st ed. Wiley, 1994.

[42] T. Moumene, E.H. Belarbi, B. Haddad, D. Villemin, O. Abbas, B. Khelifa, S. Bresson, Study of imidazolium dicationic ionic liquids by Raman and FTIR spectroscopies: the effect of the nature of the anion, J. Mol. Struct. 1083 (2015) 179–186, https://doi.org/10.1016/j.molstruc.2014.11.061.

[43] T. Moumene, E.H. Belarbi, B. Haddad, D. Villemin, O. Abbas, B. Khelifa, S. Bresson, Vibrational spectroscopic study of ionic liquids: comparison between monocationic and dicationic imidazolium ionic liquids, J. Mol. Struct. 1065–1066 (2014) 86–92, https://doi.org/10.1016/j.molstruc.2014.02.034.

[44] T. Moumene, E.H. Belarbi, B. Haddad, D. Villemin, O. Abbas, B. Khelifa, S. Bressond, Vibrational spectroscopic study of imidazolium dicationic ionic liquids: effect of cation alkyl chain length, J. Appl. Spectrosc. 83 (2016) 180–186, https://doi.org/10.1007/s10812-016-0264-7.

[45] E. Gómez, N. Calvar, Á. Domínguez, Thermal behaviour of pure ionic liquids, Ion. Liq. - Curr. State Art. (2015) 199–228, https://doi.org/10.5772/59271.

[46] B. Zhao, L. Greiner, W. Leitner, Cellulose solubilities in carboxylate-based ionic liquids, RSC Adv. 2 (2012) 2476–2479, https://doi.org/10.1039/c2ra01224c.

[47] R. Dong, P. Wen, S. Zhang, C. Zhang, W. Sun, M. Fan, D. Yang, F. Zhou, W. Liu, The synthesis and tribological properties of dicarboxylic acid ionic liquids, Tribol. Int. 114 (2017) 132–140, https://doi.org/10.1016/j.triboint.2017.04.012.

[48] A.S. Khan, Z. Man, A. Arvina, M.A. Bustam, A. Nasrullah, Z. Ullah, A. Sarwono, N. Muhammad, A. Arvina, Z. Ullah, A. Sarwono, A. Nasrullah, M.A. Bustam, Dicationic imidazolium based ionic liquids: synthesis and properties, J. Mol. Liq. 227 (2017) 98–105, https://doi.org/10.1016/j.molliq.2016.11.131.

[49] T. Mourão, L.C. Tomé, C. Florindo, L.P.N. Rebelo, I.M. Marrucho, Understanding the role of cholinium carboxylate ionic liquids in PEG-based aqueous biphasic systems, ACS Sustain. Chem. Eng. 2 (2014) 2426–2434, https://doi.org/10.1021/sc500444w.

[50] Y. Cao, T. Mu, Comprehensive investigation on the thermal stability of 66 ionic liquids by thermogravimetric analysis, Ind. Eng. Chem. Res. 53 (2014) 8651–8664, https://doi.org/10.1021/ie5009597.

[51] M. Mahrova, F. Pagano, V. Pejakovic, A. Valea, M. Kalin, A. Igartua, E. Tojo, Pyridinium based dicationic ionic liquids as base lubricants or lubricant additives, Tribol. Int. 82 (2015) 245–254.

[52] F. D'Anna, H.Q. Nimal Gunaratne, G. Lazzara, R. Noto, C. Rizzo, K.R. Seddon, Solution and thermal behaviour of novel dicationic imidazolium ionic liquids, Org. Biomol. Chem. 11 (2013) 5836–5846, https://doi.org/10.1039/c3ob40807h.

[53] T. He, Y.F. Wang, J.H. Zeng, Stable, high-efficiency pyrrolidinium-based electrolyte for solid-state dye-sensitized solar cells, ACS Appl. Mater. Interfaces 7 (2015) 21381–31390, https://doi.org/10.1021/acsami.5b06035.

[54] J.L. Anderson, R. Ding, A. Ellern, D.W. Armstrong, Structure and properties of high stability geminal dicationic ionic liquids, J. Am. Chem. Soc. 127 (2005) 593–604, https://doi.org/10.1021/ja046521u.

[55] R.M. Saeed, J.P. Schlegel, C. Castano, R. Sawafta, Uncertainty of thermal characterization of phase change material by differential scanning calorimetry analysis, Int. J. Eng. Res. Technol. 5 (2016) 405–412. https://www.researchgate.net/publication/291973182.

[56] S.O. Kasap, Principles of Electronic Materials and Devices. 2006: McGraw-Hill, McGraw-Hill, 2006.

[57] N. Calvar, E. Gómez, E.A. Macedo, Á. Domínguez, Thermal analysis and heat capacities of pyridinium and imidazolium ionic liquids, Thermochim. Acta 565 (2013) 178–182, https://doi.org/10.1016/j.tca.2013.05.007.

[58] R.D. Chirico, V. Diky, J.W. Magee, M. Frenkel, K.N. Marsh, Thermodynamic and thermophysical properties of the reference ionic liquid: 1-Hexyl-3-methylimidazolium bis[(Trifluoromethyl)Sulfonyl]amide (including mixtures). Part 2. Critical evaluation and recommended property values (IUPAC technical report), Pure Appl. Chem. 81 (2009) 791–828, https://doi.org/10.1351/PAC-REP-08-09-22.

[59] T.C. Paul, A.K.M.M. Morshed, E.B. Fox, A.E. Visser, N.J. Bridges, J.A. Khan, Thermal performance of ionic liquids for solar thermal applications, Exp. Thermal Fluid Sci. 59 (2014) 88–95, https://doi.org/10.1016/j.expthermflusci.2014.08.002.

[60] M.R. Ortega Vega, S.R. Kunst, J.A.T. da Silva, S. Mattedi, C. de Fraga Malfatti, Influence of anion chain length of protic ionic liquids on the corrosion resistance of API X70 steel, Corros. Eng. Sci. Technol. 50 (2015) 547–558, https://doi.org/10.1179/1743278215Y.0000000008.

[61] Z. Zhang, A.A.M. Salih, M. Li, B. Yang, Synthesis and characterization of functionalized ionic liquids for thermal storage, Energy and Fuels 28 (2014) 2802–2810, https://doi.org/10.1021/ef402401d.

[62] M. Armand, F. Endres, D.R. MacFarlane, H. Ohno, B. Scrosati, Ionic-liquid materials for the electrochemical challenges of the future, Nat. Mater. 8 (2009) 621–629, https://doi.org/10.1038/nmat2448.

[63] S. Mora, G. Neculqueo, R.A. Tapia, J.I. Urzúa, Thermal storage density of ionic liquid mixtures : a preliminary study as thermal fluid, J. Mol. Liq. 282 (2019) 221–225, https://doi.org/10.1016/j.molliq.2019.02.124.

[64] K. Czerniak, F. Walkiewicz, Synthesis and antioxidant properties of dicationic ionic liquids, New J. Chem. 41 (2017) 530–539, https://doi.org/10.1039/c6nj02428a.